5-2005

# New approaches in optical lithography technology for subwavelength resolution

Hoyoung Kang

# NEW APPROACHES IN OPTICAL LITHOGRAPHY TECHNOLOGY FOR SUBWAVELENGTH RESOLUTION

by

Hoyoung Kang

M.S. Hanyang University
(1987)

A dissertation submitted in partial fulfillment
of the requirements for the degree of Ph.D.
in the Chester F. Carson Center for Imaging Science
of the College of Science
Rochester Institute of Technology

May 2005

Author Hoyoung Kang Hoyoung Kang

Accepted by Name Illegible 9/1/05

Coordinator of Ph.D. Degree Program Date

CHESTER F. CARLSON
CENTER FOR IMAGING SCIENCE
COLLEGE OF SCIENCE
ROCHESTER INSTITUTE OF TECHNOLOGY
ROCHESTER, NEW YORK

CERTIFICATE OF APPROVAL

---

Ph. D. DEGREE DISSERTATION

---

The Ph.D. Degree Dissertation of Hoyoung Kang
has been examined and approved
by the dissertation committee as satisfactory for the
dissertation requirement for the
Ph.D. degree in Imaging Science

Bruce W. Smith

Dr. Bruce W. Smith, Thesis Advisor

Zoran Ninkov

Dr. Zoran Ninkov

M. Kotlarchyk

Dr. Michael Kotlarchyk

Paul Michaloski

Paul Michaloski,

9/1/05

Date

# Thesis/Dissertation Author Permission Statement

Title of thesis or dissertation: New Approach in Optical Lithography Technology for Sub Wavelength Resolution

Name of author: HOYOUNG KANG
Degree: Ph. D
Program: Imaging Science
College: College of Science

I understand that I must submit a print copy of my thesis or dissertation to the RIT Archives, per current RIT guidelines for the completion of my degree. I hereby grant to the Rochester Institute of Technology and its agents the non-exclusive license to archive and make accessible my thesis or dissertation in whole or in part in all forms of media in perpetuity. I retain all other ownership rights to the copyright of the thesis or dissertation. I also retain the right to use in future works (such as articles or books) all or part of this thesis or dissertation.

***Print Reproduction Permission Granted:***

I, HOYOUNG KANG, hereby **grant permission** to the Rochester Institute Technology to reproduce my print thesis or dissertation in whole or in part. Any reproduction will not be for commercial use or profit.

Signature of Author: Hoyoung Kang Date: May 2. 2005

***Print Reproduction Permission Denied:***

I, ~~HOYOUNG K~~, hereby **deny permission** to the RIT Library of the Rochester Institute of Technology to reproduce my print thesis or dissertation in whole or in part.

Signature of Author: _____ Date: _____

***Inclusion in the RIT Digital Media Library Electronic Thesis & Dissertation (ETD) Archive***

I, HOYOUNG KANG, additionally grant to the Rochester Institute of Technology Digital Media Library (RIT DML) the non-exclusive license to archive and provide electronic access to my thesis or dissertation in whole or in part in all forms of media in perpetuity.

I understand that my work, in addition to its bibliographic record and abstract, will be available to the world-wide community of scholars and researchers through the RIT DML. I retain all other ownership rights to the copyright of the thesis or dissertation. I also retain the right to use in future works (such as articles or books) all or part of this thesis or dissertation. I am aware that the Rochester Institute of Technology does not require registration of copyright for ETDs.

I hereby certify that, if appropriate, I have obtained and attached written permission statements from the owners of each third party copyrighted matter to be included in my thesis or dissertation. I certify that the version I submitted is the same as that approved by my committee.

Signature of Author: Hoyoung Kang Date: May 2. 2005

DISSERTATION RELEASE PERMISSON
ROCHESTER INSTITUTE OF TECHNOLOGY
COLLEGE OF SCIENCE
CHESTER F. CARLSON
CENTER FOR IMAGING SCIENCE

Title of Dissertation New Approaches in Optical Lithography Technology for Subwavelength Resolution, I hereby grant permission to the Wallace Memorial Library of R.I.T. to reproduce my dissertation in whole or in part. Any reproduction will not be for commercial or profit.

Signature Hoyoung Kang

Date May 3. 2005

NEW APPROACHES IN
OPTICAL LITHOGRAPHY TECHNOLOGY FOR
SUBWAVELENGTH RESOLUTION

by

Hoyoung Kang

Submitted to the Chester F. Carlson
Center for Imaging Science
College of Science
in partial fulfillment of the requirements
for the Ph.D. Degree
at the Rochester Institute of Technology

## Abstract

Advances in the semiconductor industry are mainly driven by improvements in optical lithography technology, which have enabled the continual shrinking of integrated circuit devices. However, optical lithography technology is approaching its limit, and within ten years, it may be substituted by new non-optical approaches. These may include Extreme Ultra Violet (EUV) lithography and charged particle beam projection lithography. While these technologies may have potentially better resolution, they can be very difficult to implement into manufacturing.

During the course of the research presented here, the extension of optical lithography to sub 70nm resolution has been investigated. Since optical lithography is mature and well understood, extending it to allow for higher resolution can dramatically reduce manufacturing difficulties, compared to EUV or charged particle beam projection lithography. A majority of the existing infrastructure, such as photoresist materials, sources, optics, and photo-masks, remain applicable with the optical methods explored here.

The avenues investigated in this research have concentrated on spatial frequency filtering in alternative Fourier Transform planes, vacuum UV wavelength lithography, and achieving ultra high numerical aperture imaging through the use of liquid immersion imaging. More specifically, novel spatial frequency filtering using angular transmission filters was developed and demonstrated. Multiple filter designs were proposed, one of

which was successfully fabricated and implemented for lithographic imaging. Spatial filtering, using angular transmission filtering, proved to enhance the resolution of contact hole images by approximately 20%. Vacuum UV imaging at the 126nm wavelength was carried out but deemed likely to be less practical for commercial viability due to source, optics, and materials issues. Immersion lithography, using the 193nm wavelength ArF excimer laser, was investigated and demonstrated for very high numerical aperture imaging. Requirements for immersion lithography were established, including the necessary design of imaging fluids, optics, sources, and photoresist materials. As a development tool, an interference lithography system was built using the 193nm ArF excimer laser and water as an immersion fluid. Patterns below 70nm were printed using the process developed, which has established the potential to extend optical lithography further than was believed at the onset of this project. This research provides proof of the concept of extending optical lithography to the 70nm generation and below.

# ACKNOWLEDGEMENTS

I would like to thank to my advisor Bruce W. Smith for his great help and opportunity to work in most advanced technology development. Discussions with him were truly helpful and inspiring for the new potential of technology. I also would like to acknowledge all of research group for discussion and help, especially Anatoly Bourov, Frank C. Cropanese, Yongfa Fan and Lena Zavyalova. Thank all the faculty and staff in Semiconductor and Microsystem Fabrication Laboratory.

I express my gratitude to Semiconductor Research Corporation for the funding of research, ASML to help printing of wafer for experiments with advanced exposure systems, Tropel for the fabrication of pupil filter and USHIO for the leasing the argon excimer lamp for long period of time.

I thank to my wife and children for their endurance and help during my studying period. Finally to my parents, I have deep appreciation for their devotion and sacrifice to raise and educate me and my siblings under most difficult situations.

Abbreviations

| | |
|---|---|
| APSM | Attenuated Phase Shift Mask |
| ARC | Anti-Reflective Coating |
| BARC | Bottom Anti Reflective Coating |
| CAR | Chemically Amplified Resist |
| CD | Critical Dimension |
| CEL | Contrast Enhancement Layer |
| CMP | Chemical Mechanical Polishing |
| COMA | Cyclo-Olefin Maleic Anhydryde |
| CVD | Chemical Vapor Deposition |
| DOF | Depth of Focus |
| DUV | Deep Ultra Violet |
| DMSDMA | Di Methyl Silazane Di Methyl Amine |
| EPL | Electron Beam Projection Lithography |
| EUV | Extreme Ultra Violet |
| HMDS | Hex Methyl Di Silazane |
| MLR | Multi Layer Resist |
| NA | Numerical Aperture |
| OAI | Off Axis Illumination |
| PEB | Post Exposure Bake |
| PHS | Poly Hydroxy Styrene |
| PMMA | Poly Methyl Metha-Acrylate |
| PSM | Phase Shift Mask |
| RET | Resolution Enhancement Technique |
| TARC | Top Anti Reflective Coating |
| TSI | Top Surface Imaging |
| VEMA | Vinyl Ether Maleic Anhydryde |
| VUV | Vacuum Ultra Violet |

Table of Contents

## List of Figures

# List of Tables

# 1. Introduction to Optical Microlithography

The improvement of optical lithography has played a very important role in the rapid development of the semiconductor industry. Both circuit speed and integration density strongly depend on the minimum printable feature size. Device yield and wafer throughput also depend on the performance of the lithography process that can make smaller chip sizes. Aside from performance issues, the economy of the integrated circuit production is also related to lithography.

Optical projection lithography has been the leading technology of VLSI manufacturing. Projection systems have evolved from longer to shorter wavelengths. The initial introduction of projection lithography used near-UV illumination, specifically the g-line of the mercury lamp. Over time, the exposure wavelength has been changed to i-line (365nm), KrF (248nm) and ArF (193nm) excimers to improve resolution. Each wavelength change has required extensive research and development. Recently, efforts focused on 157nm wavelength lithography using an $F_2$ excimer laser. 157nm lithography is expected to produce 70nm features with a number of resolution enhancement techniques. However, before 157nm lithography is viable for manufacturing technology, there are many problems that must be solved.

Some basic resolution improvement methods include increasing the numerical aperture (NA) of the projection system, utilizing a shorter exposure wavelength, and wavefront engineering, such as phase shift masking and off-axis illumination. For a higher numerical aperture, the current lens designs have already reached an NA of 0.85,

and production lenses have attained an NA of 0.75; therefore, such conventional enhancements would not afford much improvement. However, greater potential exists with immersion imaging that enables a numerical aperture greater than 1.0.

The exposure wavelength is 193nm in current high-end production. Extensive development efforts are aiming for 157nm; however, there is little room for further reduction of wavelength, though 121nm and 126nm are also candidates for future generation exposure wavelengths.

Optical lithography is approaching the limits of its capability through its very fast development. According to the International Technology Roadmap for Semiconductors (ITRS), shown in Table 1 [1], current optical lithography with 193nm will reach its limitation in 2005 with resolution at about 80nm, if there is no breakthrough. After 2007, EUV [1]-[4] or EPL (Electron Beam Projection Lithography) [5]-[7] is expected to be the manufacturing technology per the ITRS roadmap.

Table 1. Abstract of 2002 ITRS roadmap

| Year | 2003 | 2005 | 2007 | 2010 | 2013 | 2016 |
|---|---|---|---|---|---|---|
| Resolution(nm) | 100nm | 80nm | 65nm | 45nm | 32nm | 22nm |
| Via-hole(nm) | 130nm | 100nmm | 80nm | 55nm | 40nm | 30nm |
| Potential Technology | 193nm | 193nm | 193nm /157nm | 157nm/ EUV/EPL | EUV/EPL | EUV/EPL |

Extending optical lithography will have a significant impact on the future of the semiconductor industry, both technically and economically. Thus, research needs to be performed to extend optical lithography below the 70nm scale and possibly down to 35 - 40nm using spatial filtering, a shorter wavelength, and immersion lithography. Spatial filtering modifies the transmission characteristics of the projection lens using transmission and phase filters. A shorter wavelength could provide better resolution, although more extensive research and development is required. Immersion lithography enables a very high NA projection lens by filling the gap between the lens and the image with a liquid. Immersion lithography requires the study of immersion liquids and moderate changes to photo resists, projection optics, and wafer handling systems, but almost no change to the mask.

By combining these technologies, it is expected that printing below 70nm is possible with 193nm optical lithography. Further extension of optical lithography can be done with 157nm lithography.

## 2. Theory of Sub-Wavelength Optical Lithography

In considering the performance, limitations, and enhancement strategies for optical lithography, the two most important key figures of merit are the resolution (R) and the depth of focus (DOF) of the minimum printable feature size. The latter is the focal range over which the image is adequately sharp without changing in size. Both parameters are governed by Rayleigh's relations [8] - [11], as shown in Equations (1) and (2).

$$R = k_1 \frac{\lambda}{NA} \tag{1}$$

$$DOF = k_2 \frac{\lambda}{NA^2} \tag{2}$$

In the above equations, $\lambda$ and $NA$ are the exposing wavelength and the numerical aperture of the exposure system, respectively. These two quantities will be discussed in detail throughout the subsequent sections.

Rayleigh's equation (1) of the resolution limit describes the resolving power of microscope objectives and gives $k_1$ = 0.61 and $k_2$ = 1.0. In practical semiconductor lithography, $k_1$ and $k_2$ factors are generally dependent on the exposure system, resist, processes, type of the mask and patterns being imaged, as well as the requirements of the shape, and allowed range of the developed resist profile. The parameter $k_1$ can be as low as 0.25 for dense patterns, theoretically. In general, depending on the process, quality and setup of the projection system, $k_1$ can reach far below 0.5 with state-of-the-art resolution

enhancement technologies that will be discussed in later sections. The parameter $k_2$, however, is more complicated. It is generally said to be about unity. Equation (2) for the DOF is a first order paraxial approximation [13], only valid for low NA systems up to about 0.5 NA [14].

From Equation (1) the resolution can be improved in three ways: by shortening the exposure wavelength, increasing the numerical aperture *NA*, and/or decreasing the value of $k_1$. As shown in Table 2 according to the International Technology Roadmap for Semiconductors (ITRS), all three strategies have been pursued simultaneously in the past. This trend is projected to continuedin the foreseeable future.

Table 2. Trend of optical lithography system parameters

| Year | 90 | 95 | 99 | 2002 | 2004 |
|---|---|---|---|---|---|
| NA | 0.5 | 0.6 | 0.7 | 0.75 | 0.85 |
| $k_1$ | 0.7 | 0.6 | 0.5 | 0. 5 | 0.45 |
| Wavelength(nm) | 365 | 248 | 248 | 248/193 | 193 |
| Critical Dimension(nm) | 500 | 250 | 180 | 150/130 | 100 |
| Field size(mm) | 20x20 | 22x22 | 26x34 | 26x34 | 26x34 |
| DOF(μm) requirement | 1.5 | 1.0 | 0.6 | 0.4 | 0.25 |

Increasing resolution by decreasing the wavelength and increasing the numerical aperture occurs at the cost of a reduced depth of focus. With a high NA system, the DOF is reduced faster with the inverse of $NA^2$. Because of the inverse square dependency on the numerical aperture, the depth of focus becomes extremely small for high NA exposure systems. The DOF dependence on the wavelength is less severe than that on NA. Solving Equations (1) and (2) for NA yields Equation (3):

$$DOF = \frac{k_2}{k_1}\frac{R^2}{\lambda} \tag{3}$$

Equation (3) explicitly shows that a shorter wavelength affords a larger depth of focus for the same process parameters, $k_1$ and $k_2$, and the resolution, $R$. This is the motivation for exploring shorter wavelengths, even when a longer wavelength seems to be adequate. Table 3 describes calculated results of the required numerical aperture for varying wavelength and $k_1$ values to achieve 70nm resolution. In this regime, $k_1$ is expected to be about 0.35. For a lithography system to print a variety of geometries, $k_1$ needs to be higher than 0.35. Thus, to have flexible lithography, the numerical aperture should be approximately 0.97 with 193nm or 0.63 with 126nm.

Table 3. Required numerical aperture to achieve 70nm resolution

| Wavelength | $k_1 = 0.3$ | $k_1 = 0.35$ | $k_1 = 0.4$ |
|---|---|---|---|
| 126nm | 0.54 | 0.63 | 0.72 |
| 157nm | 0.67 | 0.79 | 0.90 |
| 193nm | 0.83 | 0.97 | 1.1 |

## 2.1 Improving Resolution by Decreasing Wavelength

Exposure wavelength reduction, as described in the previous section, has been executed from g-line (436nm), to i-line (365nm), to the KrF excimer laser wavelength (248nm) [14]. Each reduction brings its own issues. There were no severe issues in the transition from g-line to i-line. Minor issues included improving the transmission of the novolac photoresist and a change of the mask material to fused silica glass from any transparent glass material that was already used in g-line production. The transition to i-line did not take a long time.

The transition to 248nm required several changes. All lens materials and mask blanks were changed to synthetic fused silica glass. The light source was altered from a broad band lamp to a narrow band pulse laser because of intensity and chromatic aberration in the projection lens. There were a number of laser related problems to overcome as well, mainly optics contamination, reliability, cost, and productivity. The photoresist was changed to a chemically amplified phenolic resist, which was the most difficult issue. It took more than ten years to develop a stable chemically amplified resist. The sensitization and dissolution mechanism that was changed in the chemically amplified resist (CAR) [15] required very precise control of post-exposure bake and contamination control. Due to poor transmission of the novolac resin in g-line and i-line, the base resin was substituted with Poly Hydroxy Styrene (PHS) [16]. The porous characteristics of PHS generated another set of chemical contamination problems [17].

The industry transition to 193nm lithography has recently begun. Two major changes in the 193nm system are the introduction of $CaF_2$ crystal lens elements and a new resist polymer. The traditional lens materials were not transparent with exception of synthetic fused silica, however, it degrades in a short period of time with a high pulse dose [18] - [20]. Thus, $CaF_2$ has to be used in high dose applications such as in the region of the illuminator and the last few elements of the projection lens [21] - [22]. In the photoresist, the base resin of the chemically amplified resist had to be changed again to a more transparent polymer at 193nm. Poly Hydroxy Styrene (PHS) used in 248nm lithography, is not transparent to 193nm. Still, a number of different polymers [23], such as VEMA (Vinyl Ether Maleic Anhydryde), COMA(Cyclo-Olefin Maleic Anhydride), and multiple derivatives of PMMA (Poly Methyl Metha-Acrylate) have been suggested and exercised. None of these show characteristics as good as PHS at 248nm.

Due to the rapid development of KrF lithography, it is likely that 193nm exposure systems were introduced with a 0.75 NA to production with the use of RETs (Resolution Enhancement Technique). 193nm lithography can provide a solution for sub-100nm technology but not for every type of pattern. Some patterns, like via-holes, require a very strong miniaturization technique, even with 193nm lithography for the sub-100nm generation.

Recently, lithography at the 157nm wavelength of the F2 laser has been pursued. One of the few known optical materials capable of transmitting 157nm laser radiation [24] - [28] is $CaF_2$ crystal, which has insufficient optical quality and an inadequate

infrastructure to fabricate large enough sizes and quantities to support the lithography requirement. Other transparent materials such as Magnesium Fluoride have unacceptable intrinsic birefringence [29] and Lithium Fluoride, which is relatively soft and hygroscopic, was also excluded. In addition to the material problem, the $F_2$ excimer laser was not mature yet.

Significant advances have recently been made enabling the technology. Both the $F_2$ laser and $CaF_2$ material development have progressed greatly in the last few years. A laser capable of a 600Hz, 6 Watts output has been demonstrated with remarkable improvement with its 2pm bandwidth. However, this bandwidth only allows only catadioptric lens system; otherwise the lens will suffer from chromatic aberration. Still, there are many fundamental challenges in 157nm lithography that are listed and discussed in Section 5.1. These include birefringence issues with $CaF_2$ [27], the lack of a suitable mask [30], mask pellicle materials [31] - [32], and the need for new photoresist materials development [33] - [37].

## 2.2 Resolution Enhancement Techniques

Resolution Enhancement Techniques (RETs) modify the shape of the wavefront of an imaging system at the illumination pupil and/or the imaging pupil by spatial filtering [38]. Some RETs are very similar to those used in microscope technology.

Several approaches have become promising for application in optical lithography. Examples of optical RET include phase shift mask technology, off-axis illumination (modified illumination), and spatial frequency filtering.

### 2.2.1 Off-Axis Illumination (OAI)

Off-axis illumination is a common RET method at the illumination plane. The illumination coherence in the spatial domain is an adjustable parameter that has influence on the imaging performance. The illumination is said to be partially coherent if a certain amount of spatial coherence exists. The amount of partial coherence is governed by the ratio of the numerical aperture of the condenser lens ($NA_i$ ) to the projection lens ($NA_o$). The so-called partial coherence factor, $\sigma$, is shown in Figure 1.

The influence of coherence is demonstrated by simulation in Figure 2 by showing the image intensity near a simple knife-edge [38] - [40]. The limiting case $\sigma = 1$ corresponds to incoherent illumination that gives the smoothest profile. Decreasing the coherence increases the edge slope, which decreases the intensity minimum near the edge on the bright side. The local maximum intensity on the dark side of the pattern and minimum intensity on the bright side determine the line edge fidelity and profile quality. If $\sigma$ is reduced to values as low as 0.1 in order to decrease the intensity minimum, the intensity ringing becomes excessive and extends laterally. The limiting case $\sigma = 0$ refers to an ideally coherent point source yielding the sharpest slope but intolerable overshoot. In practical lithography, typical sigma value ranges between 0.3 and 0.8.

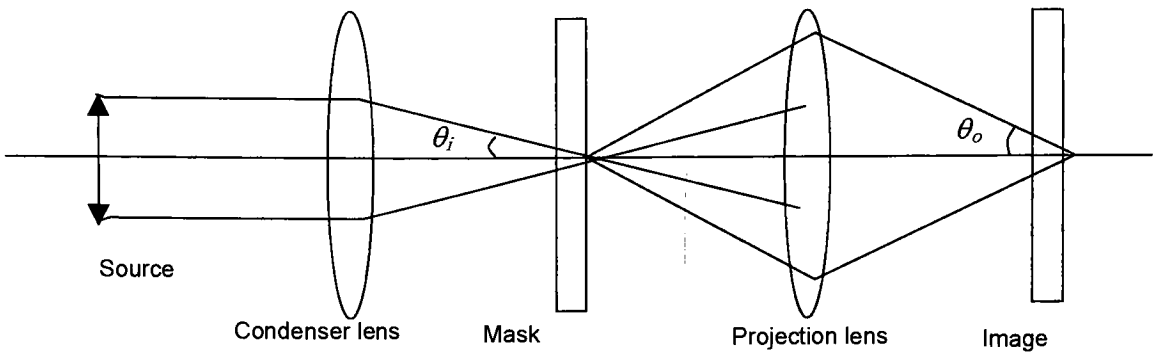


$NA_o = sin\ (\theta_o)$ where $\theta_o$ is half angle at image
$NA_i = sin\ (\theta_i)$ where $\theta_i$ is half angle at source
$\sigma = Na_i / NA_o$

Figure 1. Definition of NA and coherence factor σ in a Koehler Illumination system

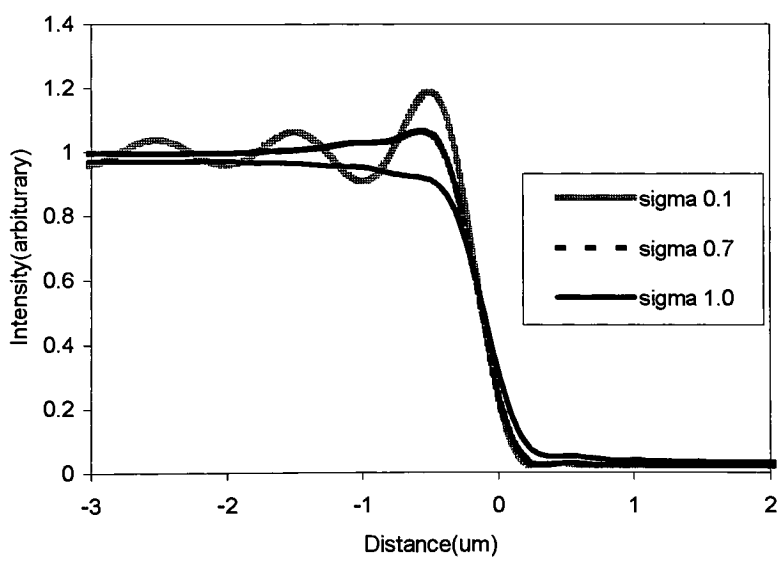


Figure 2. Image profile at the edge of pattern with different coherence factor

An aperture is introduced in front of the light source to control the coherence factor. This aperture changes the effective size of the source. A circular aperture, as in the case of partially coherent illumination, refers to simple low pass filtering with a cut-off frequency determined by the numerical aperture of the condenser lens ($NA_c$) and that of the projection lens. Only plane waves up to a certain amount of obliqueness can pass through the mask.

By applying only oblique illumination, it is possible to change the minimum period of pattern whose first diffracted beam can pass through the projection lens. The zero order beam will pass through the edge of the projection lens, thus the minimum resolvable period $R_c$ [41]is given by Equation (4)

$$R_c = \frac{\lambda}{NA(1+\sigma_{offset})} \tag{4}$$

where $\sigma_{offset}$ is angle of obliqueness in terms of $\sigma$

Equation (4) only gives the minimum resolvable period and not the real resolution. When only an oblique beam is utilized with $\sigma_{offset}$ and proper resist, resolution can be achieved as per Equation (4). By applying this principle, depending on the chip design and resolution requirement, an annular aperture or multipole aperture can be used. Aperture shapes and applications are depicted in Figure 3.

The annular aperture has no directional preference; however, there will be more zero order light than first order, thus creating low contrast. The quadrupole aperture has a preference for the vertical and horizontal directions but has a higher contrast than the

annular aperture and a lower cut-off frequency. The dipole aperture can have the highest resolution and contrast but is effective only for one directional pattern. There is potential for completely customized illumination for a specific pattern whose application is limited to the regular array of very dense patterns [42].

The downfall of off-axis illumination is that it always rejects one side of the diffracted light to attain higher resolution. The image contrast for a nominal resolvable pattern is much lower than that of conventional illumination. This is the reason why this technique was not applied previously, even though it was well known in the optics field. Low contrast images generated by off-axis illumination can be printed with the improvement of photoresist contrast.

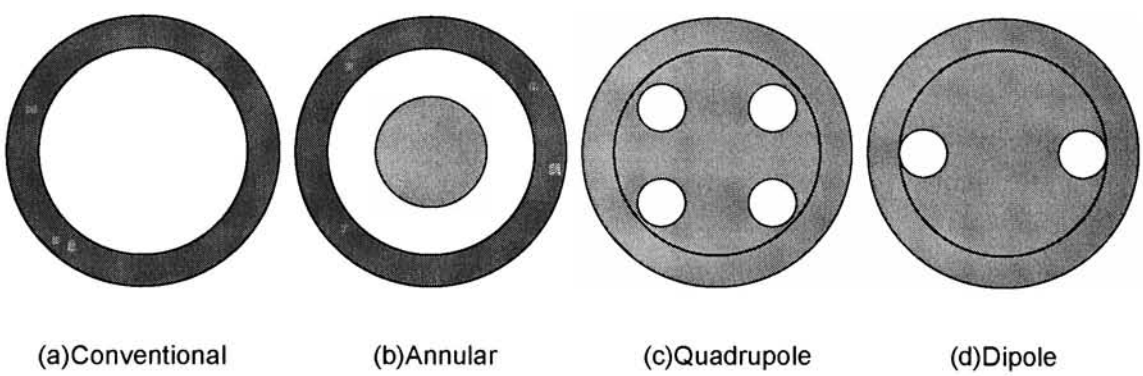


Figure 3. Various aperture pupil diagram

In off-axis illumination, when the zero order and first diffracted order are well chosen, both beams may have the same angle from the vertical, and there is no phase difference between the two beams even with defocus. The DOF of periodic features may be infinite in theory. For this reason, modified illumination schemes, or "off-axis"

techniques, have become a well-established method extending optical lithography towards sub-wavelength resolution. In physical situations, the DOF may not be infinite because of the finite size of the illumination source, the area of repeating pattern, and lens aberrations.

### 2.2.2 Phase Shift Mask Technology

Due to their binary nature, conventional binary masks either transmit or attenuate light without varying phase. Adding a phase-shifting function to binary masks may yield a higher resolution at the same or larger depth of focus. Thus, phase-shifting is a technique used to reduce the $k_1$ parameter [44]. The enhancement is defined from the fact that both the amplitude and phase are used to store information about the image on the mask.

The phase-shifting principle was first introduced in 1982 by Marc Levenson, but has since remained as a development technology. Recent enormous efforts have been made in industrial applications and production application has begun for special applications [47].

There are several different types of phase shift masks. The various types of masks are presented in Figure 4. Among them, alternating phase shift masks in (b), the phase edge masks, and attenuated phase shift masks in (d) [48] - [50] are the most interesting in practical application.

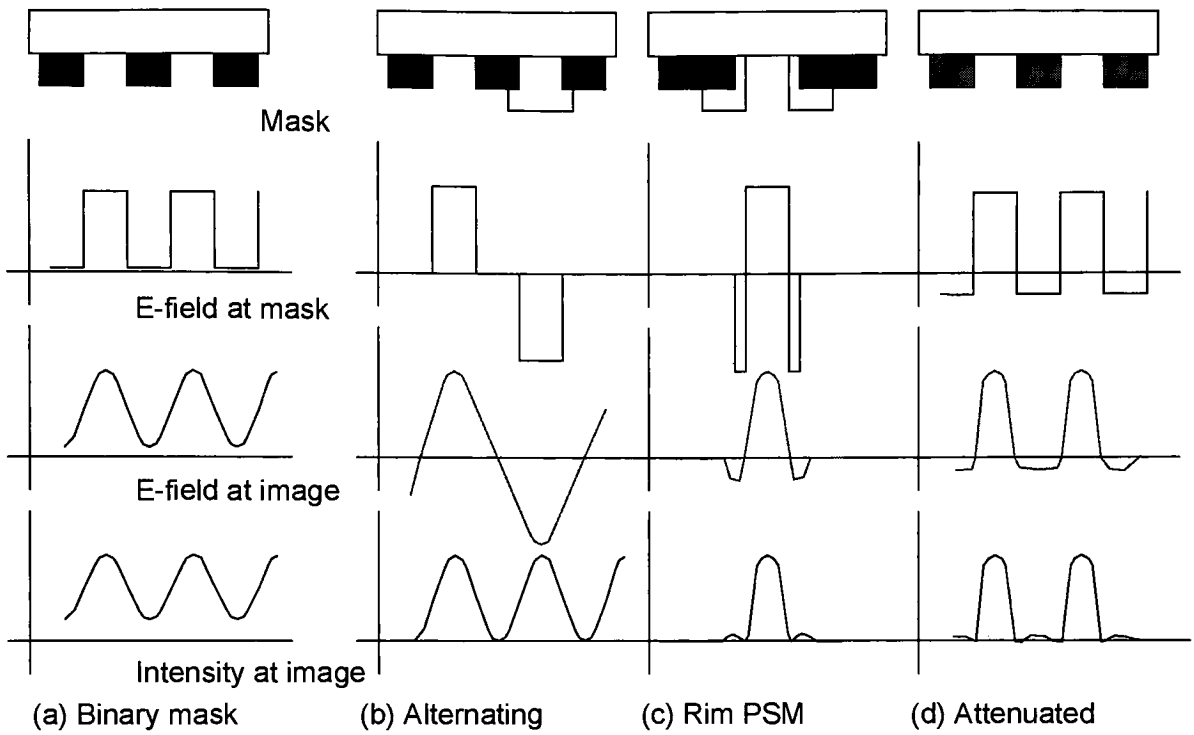


Figure 4. Various types of phase shift masks

An alternating type of phase shift mask or phase edge mask in Figure 4(b) has a phase for each of the two clear patterns. Two periods of lines and spaces have only one period when phase is included. The resulting diffraction pattern does not contain zero and even orders, and first order diffracted light appears at half of the angle of the binary mask. There are only two equally powered first orders in the pupil for a small period pattern. When it is imaged on the imaging plane, there should be a point that has zero intensity in the dark area. This feature makes it easier to print a very fine line, but not a fine space, with positive resist. Application of the alternating type mask requires a very wide area in

the layout to solve the phase conflict that cancels the merit of phase shift masks. Another approach to solving the phase conflict is by using a secondary mask to remove conflict areas. This method reduces some of the merit of phase shift mask although there are some possibilities of improving lithographic productivity. Printing very fine features with relatively wide pitch became an easy task using this method.

When a feature is isolated from other patterns, a narrow area with opposite phase may be added to improve the contrast of the image, as shown in Figure 4(c). The attenuated phase shift mask in Figure 4(d) has a different application. Combined with various illumination techniques, it may be used for almost all kinds of patterns. The attenuated phase shift mask has an ranges of 5 – 20% transmission leak in the dark area with a 180° phase change relative to the clear area. In general, it was developed for imaging via-holes. Because of the phase difference near the pattern, the intensity at the edge of the via-hole pattern goes to zero and the via-hole image narrows. In principle, attenuated phase shift masks reduce the zero order intensity. This works well with dense line and space patterns by reducing the zero order beam intensity relatively, combined with off-axis illumination.

### 2.2.3 Spatial Frequency Filtering

Spatial frequency filtering is an image processing technique applied in the spatial frequency domain. A recently proposed method referred to as in-lens filtering enhances the depth of focus by placing a special amplitude and phase filter in the pupil plane of the projection lens [51], which functions as the spatial frequency plane. However, pupil plane

filtering has primarily been of theoretical interest in microlithography since the pupil plane in lithographic lenses is usually not accessible to the user unless the lens is disassembled. Furthermore, different mask types require different types of spatial filtering for optimum performance. Thus, the in-lens filter cannot simply be a fixed optical element, which makes this approach hardly practical in manufacturing processes where a large number of different mask patterns are applied during the fabrication process of an integrated circuit.

## 2.3 Improving Resolution by Increasing Numerical Aperture

Increasing the numerical aperture [52] may directly improve resolution by increasing the cut-off frequency in the spatial domain, as in Equation (1). However, increased numerical aperture can reduce the depth of focus. Rayleigh's equation (2) on the depth of focus is a paraxial approximation for low NA. It can be modified to account for high NA lithography imaging [53]:

$$DOF \leq \frac{\lambda}{8\sin^2(\theta/2)} \tag{5}$$

where $NA = \sin\theta$. From Equation (5), it can be easily seen that higher numerical aperture reduces the depth of focus faster than the original Rayleigh's equation (2), so the merit of increased numerical aperture is reduced more abruptly in depth of focus.

Another problem in increasing numerical aperture is an economic issue. Increased numerical aperture requires more complex lens designs and fabrication that is already highly complicated [52]. Current high-end lens designs have very high NA's on the order

of 0.85. Further increases in NA do not give much improvement in resolution with respect to the cost and challenges [54].

# 3. Overview of Experimental Approach: Research into Sub-Wavelength Optical Lithography

Research to extend optical lithography technology beyond 70nm covers broad spectrum. Several basic approaches are mentioned in the previous chapter. Among the resolution enhancement methods described in Chapter 2, a study was carried out in three major areas including spatial filtering, shorter wavelength exposure with 126nm, and the potential of very high numerical aperture with liquid immersion.

## 3.1 Spatial Filtering Outside of the Lens Pupil

The wavefront traveling in the optical system may be modified through spatial filtering as described in Section 2.2.2. Spatial filtering in projection lithography is essentially used as a high pass filter. High pass filtering in Fourier optics is a well-known technique. The difference between lithography and image processing is the resolution and contrast requirement. Lithography requires printing high contrast images near the limits of optical imaging.

Spatial filtering may be done by inserting an amplitude and phase filter in the pupil of the projection lens. Through spatial filtering, resolution and image profiles may be modified. However spatial filtering in lithography is prohibitively difficult because of the complexity of the projection lens. The pupil plane is barely accessible because it is in the most critical part of the optical system. Therefore, filters should have good optical

characteristics including flatness, thickness, and proper positioning. They should not generate any heat from light absorption, which can change the quality of the optics. Filtering requirements are also different from pattern to pattern, so the filter should be easily exchangeable. These requirements are not easily achievable with a conventional system.

An alternative approach for spatial filtering suggested in this study is to carry out the spatial filtering at an alternative pupil plane, specifically, near the mask or image plane. These locations correspond to spatial frequency planes of the mask and image field but exist at an angular distribution of diffraction. Theoretically, angle-dependent transmission filtering (angular filtering), near the mask or image, is the same as transmission and phase in the spatial filtering of the pupil. The position of the angular filter may be located near the mask, just outside of the Fraunhofer region, a distance greater than $R^2/\lambda$, where R is the range of mask pattern that carries as Fourier transform. When an array of via-holes near the resolution limit is illuminated with nearly incoherent illumination, Fraunhofer approximation distance is about the size of a via-hole. With partially coherent illumination, the distance should be increased with the inverse of the coherent factor. A few microns are sufficient for 193nm lithography considering the pattern, resolution, coherence of illumination, and wavelength. Therefore, the filter may be located at the pellicle [55] plane, which is about 6mm from the mask, in place of the mask pellicle. A pellicle is a thin, transparent membrane spaced several millimeters away

from the mask on an aluminum frame to prevent particles from degrading the mask image performance by contamination.

A study of alternative spatial filtering, optimization of imaging via-holes, design and fabrication of an angle dependent filter, and lithographic evaluation was carried out.

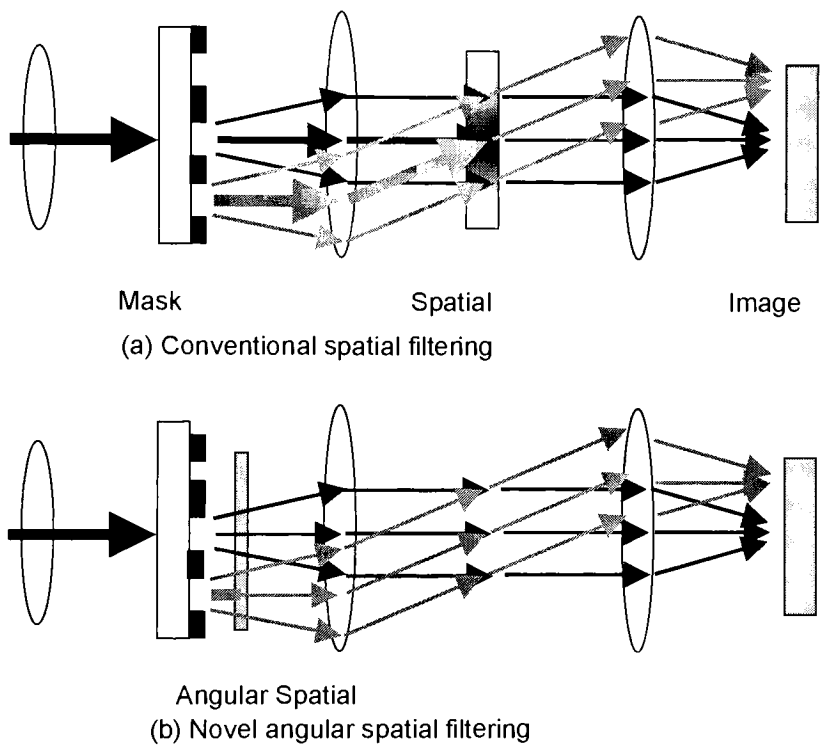


Figure 5. Conventional and novel spatial filtering technique diagram

## 3.2. Optical Lithography at 126nm Wavelength

In Rayleigh's equation, a shorter wavelength will result in better resolution for a given numerical aperture, or a better DOF for a given resolution. That is, if the same or a

similar NA can be achieved, a shorter wavelength will give better resolution. Thus, it is reasonable to study wavelengths shorter than 157nm for future generations.

An extreme case of a shorter wavelength is EUV. The EUV wavelength that is applied to lithography is 13.54nm. It potentially has 15 times the capability over current 193nm lithography. However, there are a number of difficult issues, such as a defect-free reflective mask, a bright and clean source, high NA projection optics fabrication, and the lifetime of optics.

Rather than the dramatic change in wavelength to EUV, there are other more plausible wavelength choices available. Potential wavelengths include 126nm and 121nm. These wavelengths offer about 20% resolution improvement over the 157nm wavelength, which is similar to the improvement in the transition from 193nm to 157nm.

To evaluate the potential of 126nm lithography, paper studies for proper materials and a light source have been carried out. In addition, a small field Schwarzschild objective lens was evaluated for a research exposure system and a small field exposure apparatus was built, and utilized for imaging experiments.

## 3.3. Higher Numerical Aperture through Liquid Immersion Lithography

An alternative approach to shorter wavelength is the use of a high refractive index fluid between the imaging lens and the image. The high index fluid effectively reduces the wavelength by a factor of the refractive index. For 193nm lithography, commercial

lithography equipment manufacturers have already announced that 0.85NA exposure systems are near the maximum numerical aperture for conventional systems. As described earlier, higher numerical apertures will allow higher resolution. Lithography lenses are currently produced with 0.75NA, while lenses with 0.85NA are being developed. Further increases in NA are not practical because of a loss in DOF and the prohibitively high cost of the lens[56].

The numerical aperture can be much greater than unity with less of a reduction in the depth of focus when a liquid immersion system [57] - [63] is considered. However, the theoretical limitation of the numerical aperture is near the index of the liquid used for the immersion fluid because the wavelength in the liquid scales with $\lambda / n$. For example, the wavelength in water is 134nm when it is applied to 193nm.

Immersion imaging techniques have been widely used in optical microscopy. In 1880, Hugh Powell made the first 1.5NA apochromatic oil immersion microscope. Carl Zeiss of Jena, Germany, produced the first oil immersion objective in 1880, designed by Ernst Abbe, who was the founder of the optical theory of microscope lenses. Imaging in a high index fluid is a well-known technique in optical microscopy. In fact, many studies of liquid immersion microscopy were conducted in the early 20th century to improve resolution. Unlike microscopy, lithography was limited to dry imaging until now. This was mainly due to the difficulty of handling liquid in a mass production environment, which is unlike the research environment of microscopy. The high index oil that can yields improvement in resolution with a longer wavelength is especially difficult to

handle. Instead of using immersion technology, lithography used a direct reduction in wavelength. Moreover, lithography was limited in the region of relatively low NA until recently, and longer wavelength resist material was not compatible with liquid immersion [61]. However, further reduction of wavelength may affront fundamental physical problems. It has become necessary to try liquid immersion to reduce the effective wavelength or increase the numerical aperture.

When the imaging medium is not air or vacuum, the depth of focus equation (2) should be modified to include the index of the medium as in Equation (6).

$$DOF = k_2 \frac{\lambda n}{NA^2} \tag{6}$$

For high NA systems, Equation (6) should be modified accordingly:

$$DOF \leq \frac{\lambda}{8n\sin^2(\theta/2)} \; ; \tag{7}$$

where $NA = n\sin\theta$ is the definition of the numerical aperture that includes the index of refraction. The index changes the optical path difference linearly. Lithography in the high index medium can have a higher depth of focus, as in Equation (6) and Equation (7), for the same resolution capability. For the same NA, imaging in a high index medium can improve DOF, while a higher NA system can improve resolution.

Cryogenic noble gas liquids [62] and fluorinated solvents are candidates for immersion liquid, and have been suggested for 157nm wavelengths and below. Fluorinated solvents that have been evaluated by Switkes et.al [63] are still quite opaque

at 157nm. Because of the low transmission and low index of fluorinated solvents at 157nm in addition to the difficulty of 157nm imaging, it is very difficult to realize liquid immersion lithography with 157nm.

Water is a good candidate as an immersion liquid for 193nm lithography. Water is relatively well characterized and compatible with the existing process at 193nm resist materials. The refractive index of water [64] remains relatively low for longer wavelengths, although, it increases as it reaches the absorption boundary. At 193nm, the refractive index reaches up to 1.437, which grants 44% resolution improvement. If water exhibits good transmission and index characteristics at 193nm, it will be the most practical liquid for immersion lithography.

There are a number of issues that arise with immersion lithography. One of the most obvious challenges involves the handling of wafers and the resist in the liquid. A mechanical apparatus can be designed to accommodate the immersion liquid in the vicinity of projection while keeping other areas dry. This is merely a technical issue not a fundamental physical barrier. A simple conceptual drawing in Figure 6 is suggested for this study [61] - [65]. Clean water is supplied from one side of the lens and drained through the other side. The surrounding air curtain will hold water only under the lens. Another possibility is to immerse the whole wafer in a small water bath on the wafer stage thus the whole stage moves with the water bath [66]. The latter method is possible, but the former is more practical because of a lighter stage weight that enables higher throughput.

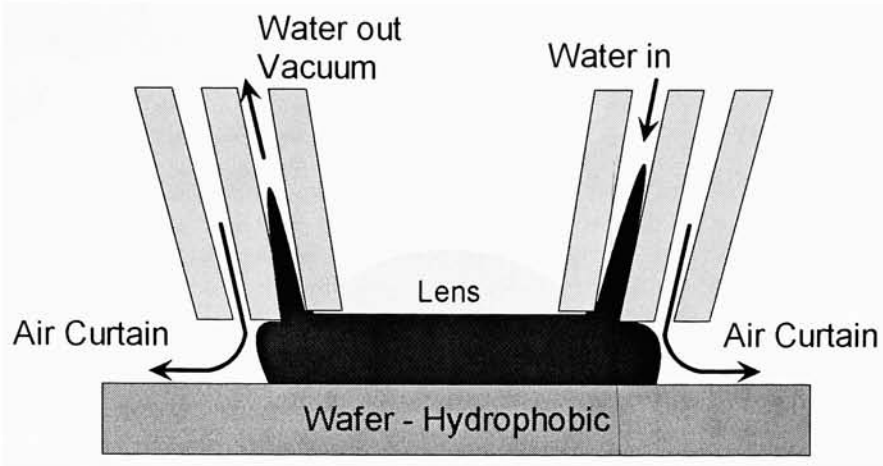


Figure 6. Immersion fluid flow diagram for stepper or scanner

Problems that need to be investigated in immersion lithography include index variations of the immersion liquid with temperature, pressure, wavelength, micro/nano-bubbles [68] in liquid, and resist-water interactions. Index variation with wavelength can simply induce a chromatic aberration [69] because the immersion liquid itself is a refracting medium. The thickness of the liquid is expected to be a few millimeters; therefore, color dispersion in this region should be much smaller than the depth of focus.

Studies were concentrated to characterize the requirements of the immersion liquid and the properties of water, resist, and the water interaction. As proof of the concept of technology, a modified Talbot interferometer has been developed. Finally, a 90nm pitch pattern was printed with immersion interference lithography.

# 4. Sub-Wavelength Optical Lithography Part 1: Spatial Filtering outside of the Lens Pupil

Spatial filtering technique is useful for high resolution imaging. Specially, via hole image is very useful application. Imaging of via is optimized based on coherent imaging system. Angular spatial filters have been designed and fabricated and exercised with projection imaging system.

## 4.1 Optimization of the Pellicle Plane Spatial filter

A particularly useful application for spatial filtering is in the imaging of small via objects known as contact holes. The optimized shape of the spatial filtering function for these via-hole features is discussed. Imaging of via-holes with a coherent source can be explained with Fourier Transformation analysis [70] - [71]. When a mask has the square via-hole size $a$ and the wavelength is λ, the electric fields at the mask $m(x, y)$ and at the pupil $M(u, v)$ are as follows:

$$m(x,y) = Rect(\frac{x}{a}, \frac{y}{a}) \tag{8}$$

$$M(u,v) = \frac{i}{R}\iint m(x,y)e^{-2\pi i\frac{xNAu+yNAv}{\lambda}}dxdy \tag{9}$$

$$M(u,v) = ASINC(\frac{aNAu}{\lambda}, \frac{aNAv}{\lambda}) \tag{10}$$

where $A$ is amplitude factor including all factors affecting intensity, and x/y are spatial coordinates in the mask plane and $u/v$ are the corresponding spatial coordinates in the frequency domain .

The pupil image has a SINC function shape. Near the resolution limit, the pupil width is much smaller than the width of the SINC function, therefore the filtered pupil image is nearly a cylindrical function rather than the intended SINC function. The field intensity at the center of the pupil is much higher than at the edge of the pupil. The field amplitude is calculated in Table 4. The pupil image is filtered with the pupil aperture and the final image is the inverse Fourier transformation of the pupil image. Control of the pupil image will change the final image size and shape. A narrower pupil image will make wider final images. Reduced intensity at the pupil edge will also result in a wider final image. If we can make the pupil image constant across the pupil or lower intensity at the center of the pupil related to the cylinder function, the final image will be narrower than that of a normal imaging system.

When a via-hole mask is illuminated with coherent light, the pupil function and the image profile is described by the following equations:

$$M(u,v) = \frac{i}{R}\mathrm{sinc}(\frac{aNAu}{\lambda}, \frac{aNAv}{\lambda}) \tag{11}$$

$$M'(u,v) = \frac{i}{R}\mathrm{sinc}(\frac{aNAu}{\lambda}, \frac{aNAv}{\lambda})Cyl(\frac{\sqrt{u^2+v^2}}{NA}) \tag{12}$$

$$m'(x,y) = B\,\mathrm{Rect}(x/a, y/a) * \frac{\mathrm{J}_1(aNAr/\lambda)}{NAr/\lambda} \tag{13}$$

$$I(x,y) = B^2 \,\mathrm{Rect}(x/a, y/a) * \frac{\mathrm{J}_1{}^2(aNAr/\lambda)}{NAr/\lambda} \tag{14}$$

Where $B$ is an amplitude factor including all factors affecting intensity, $M'(u,v)$ is the electric field in the pupil, $m'(x,y)$ is electric field in the image plane, r is $\sqrt{u^2+v^2}$, and $I(x,y)$ is the intensity profile at the image plane.

For a given lens and wavelength without any spatial filtering techniques, the image profile of the smallest via-hole is the square of the 1st order Bessel SINC function (BESINC, $\frac{\mathrm{J}_1(\rho)}{\rho}$ ) of dimension of $NAr/\lambda$, when the hole size in the mask is infinitesimal. The BESINC function has a tail and side lobes with infinite support, therefore the images can not be smaller than the original mask size.

The proper transmission function in the lens pupil can transform the Fourier transformed image into the defined flat cylinder function with reduced intensity. The electric field at the edge of the pupil and the required transmission to make a flat cylindrical intensity profile at the pupil are summarized in Table 4 for a 0.7NA 248nm system.

Table 4. Normalized E-field at the edge of lens pupil for 0.7NA DUV

| Via-hole Size (nm / $\lambda/NA$) | E-field intensity At edge of pupil |
|---|---|
| 250nm / 0.7 | 0.37 |
| 200nm / 0.56 | 0.55 |
| 180nm / 0.50 | 0.62 |
| 160nm / 0.45 | 0.70 |

Further reduction of the image size can be done with a loss of intensity and a side lobe that appears outside of the desired pattern. If we can add a small negative intensity of 2-besinc functions at the edge of the original impulse response function, which is BESINC($NA\ r/\lambda$) the image can be narrower than one with the original impulse function as shown on Figure 8. Equation (15) represents the pupil function with the inverse cosine profile where $r$ is the relative radius in the pupil. The resulting image adhere to Equation (16). The modified pupil function is shown in Figure 7. Images of the related Fourier component are displayed in Figure 8. The resulting image using the cosine pupil is displayed in Figure 9 compared to the normal image. There is higher intensity in the sidelobe that should be optimized depending on the resist contrast and pattern density.

$$M'(r) = E_0\{1 - b\cos(\frac{\sin r}{NA})\}Cyl(\frac{\sin r}{NA}) \tag{15}$$

$$m(x,y) = E_1\{\delta(r) - b\delta(r - \lambda/NA) - b\delta(r + \lambda/NA)\} * \text{Besinc}(NAr/\lambda) \tag{16}$$

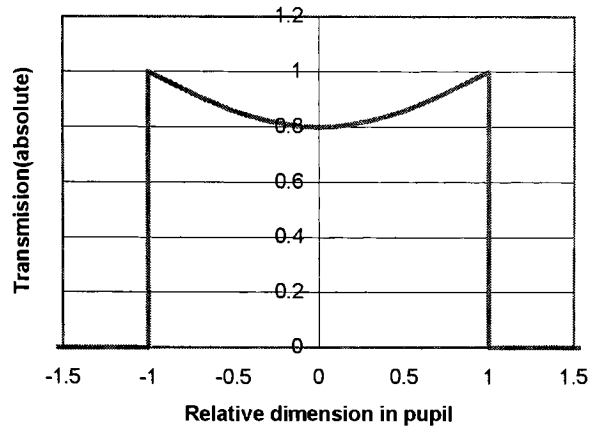


Figure 7. Profile of inverse cosine pupil

In Figure 9, the full width at half maximum (FWHM) of the inverse cosine pupil image is 17% smaller than the original SINC image generated by a perfect cylindrical pupil image.

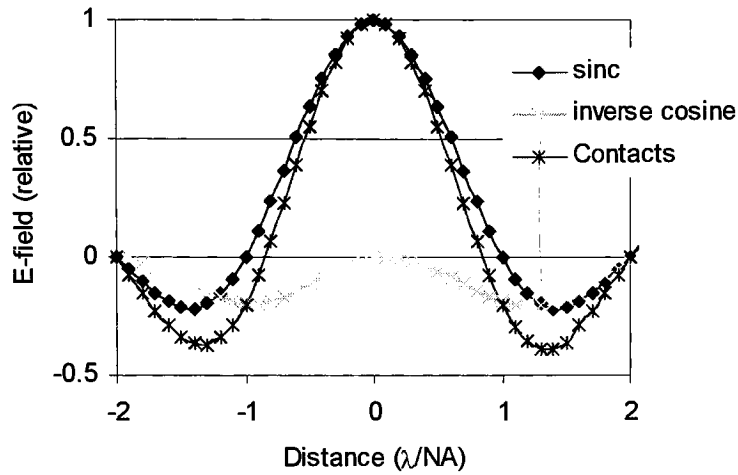


Figure 8. Electric field distribution with inverse cosine pupil intensity

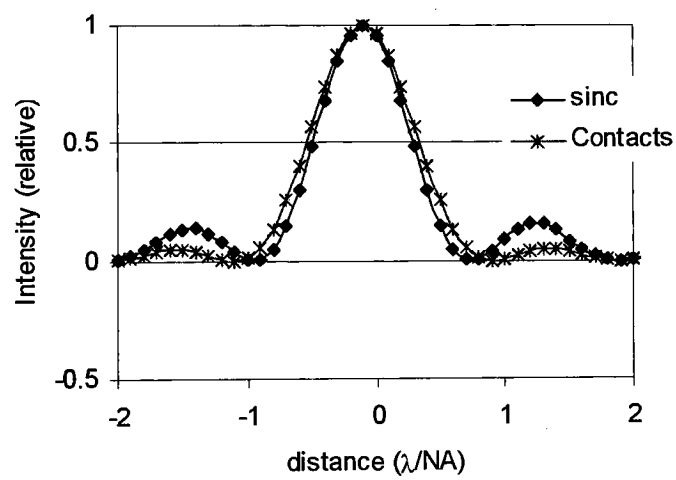


Figure 9. Image profile comparison between contact using inverse cosine pupil and sinc image

## 4.2 Design of the Angular Spatial filter

As an alternative approach to conventional spatial filtering techniques [72] -[73] a spatial filtering technology can be implemented with angular transmission characteristics. The angular transmission filter can be made using multilayer thin film techniques. In the multilayer thin film angular transmission filter, the thickness variation across the filter affects the transmission, but does not generate wavefront aberrations since the spatial plane of projection lens pupil is related to the angle at the filter and does not generate heat from absorption inside lens.

The system used for this design study was a projection system with a 0.7NA, 4X magnification 248nm wavelength, and a target via-hole size of about 0.25μm or smaller. A filter must be designed that has the lowest transmission at the vertical incidence and the highest transmission at the angle of $\sin^{-1}(NA)$). The NA at the mask side is smaller than that of the image side by a factor of the magnification. Thus, at 0.70 NA with a 4X magnification, the highest transmission angle should be 10° for a 4X system.

The Fourier transformed image function of a via-hole near its resolution limit which is about 180nm, has a 62% at the edge of the pupil relative to the center of pupil electric field intensity. The filter designed should have 62% transmission at normal incidence and 100% transmission at 10°.

To make this type of angular transmission filter, a low finesse Fabry-Perot etalon [74] was used. A low refractive index material, sandwiched between high refractive index materials, is one design option. The thickness of the low refractive index material may be

slightly thick for a pellicle based coating compared to the normal optical coating which makes it difficult to fabricate. The minimum transmission at the normal incidence can be limited by the index of available coating materials and obtainable thickness. The thin film design software Tfcalc [tm], by Software Spectra Inc. [75], was used for several variations of the filter design

### 4.2.1 Design Approach 1 – Organic Film based on Fabry-Perot Designs.

One approach to the filter design is through the alteration of an existing organic pellicle material made up of a polymer film. The nominal thickness of the pellicle film is on the order of 1 micron. The fluoro-polymer pellicle based material has a low index near 1.4. However, there was no proper high index organic coating material available for 248nm. If it is possible to apply on inorganic coating material, there are several materials that can be used. As a high index coating material $Al_2O_3$ was evaluated for the design. A high index inorganic coating on both sides of fluoropolymer pellicle can make a good angle dependent filter, as shown in Table 5 and Figure 10. This filter can results in 73% transmission at the vertical incidence, which is slightly higher than the target transmission. Higher index materials give even lower transmission. This design is feasible, however, alternative inorganic approaches were pursued.

Table 5. Single coating pellicle filter design

| Material | Thickness | Index |
|---|---|---|
| $Al_2O_3$ | 31.20nm | 1.7136 |
| Fluoro-polymer | 2767nm | 1.403 |
| $Al_2O_3$ | 31.20nm | 1.7136 |

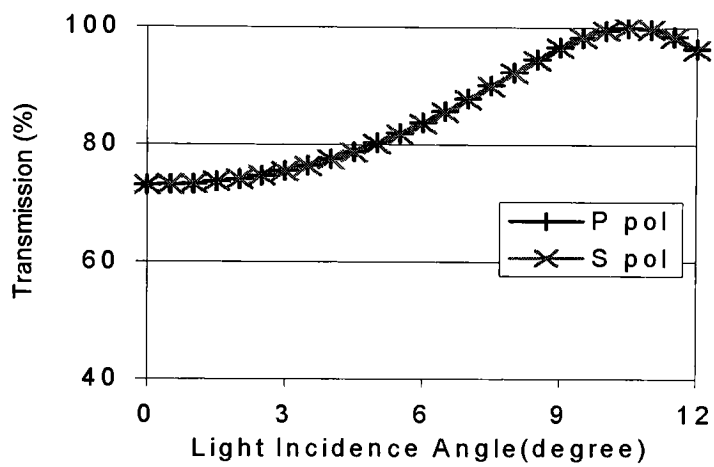


Figure 10. Transmission of fluoropolymer based single layer coating DUV filter

## 4.2.2 Design Approach 2 – Inorganic Layers based on Fabry-Perot Designs.

Another possible approach for a thinner coating is an etalon with a multi-layered coating for higher reflectance. Higher reflectance gives even stronger angular variation of transmission. In a high finesse Fabry-Perot etalon, very low transmission at normal incidence can be obtained. Thus, the center layer can be thinner than the previous design, even with the higher index of the center layer material.

The design that was actually fabricated and used for the exposure has a 3-layer coating on a glass substrate as a simplified form of the multi-layer design, which is shown in. A transmission of 73% at normal incidence was achieved in this design. The maximum transmission difference between normal and oblique incidence can be obtained at the thickness that gives 0.25° phase difference between the normal and oblique incidence. That thickness is generally too thick to fabricate, so it was necessary to trade off between thickness and thickness control. The transmission characteristics of the designed filter are shown in Figure 11. When both sides of the filter are coated, it was possible to have below 60% transmission at the normal incidence. Using the double sides coating the lithographic performance can also be enhanced.

Table 6. Filter design on fused silica substrate

| Material | Thickness | Index |
|---|---|---|
| HfO2 | 31.8nm | 2.38 |
| SiO2 | 2548nm | 1.509 |
| HfO2 | 41nm | 2.38 |
| silica substrate | 0.25mm | 1.509 |

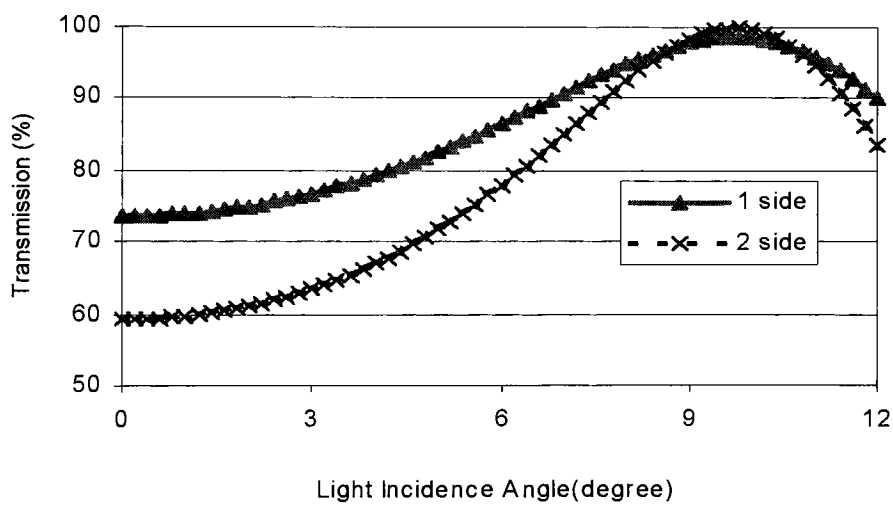


Figure 11. Transmission of designed filter on fused silica substrate

### 4.2.2 Potential Problems of Fabry-Perot Designs

A plane parallel plate can change the phase between the normal incidence and oblique incidence. The phase difference is about as shown in Equation (17) where $\theta$ is incidence angle and thickness is thickness of sandwitched layer.

$$Phase\_Difference = thickness * (1 - 1/\cos(\theta)) \tag{17}$$

Multiple reflections can generate different phases. Still the phase difference between the normal incidence and oblique incidence is very similar to plane parallel plate because the intensity of multiple reflected light of which intensity is about 30% of normal incident light is weak compared to directly transmitted light.

The phase difference induced by plane parallel plate is very similar to defocus at low angles. As incidence angle increase, it will include a higher order term, which will correspond to spherical aberration. Thus, when we use this filter with very high angles like a 1x high NA lens, compensation for spherical aberration is required. With pellicle plane filtering, the maximum angle is about 10° with a 0.7NA, and 4x magnification system. Thus, only the focus calibration is necessary even with the thick glass pellicle filter.

## 4.3. Fabrication of Spatial Frequency Filters

A pellicle plane filter was fabricated with a 3 layer coatings on a fused silica substrate with design 2. The coating material was evaporated with an e-beam assisted evaporator, while thickness was monitored with a quartz crystal micro balancer.

Transmission was measured with a spectroscopic ellipsometer, as shown in Figure 12. The surface reflection was compensated with the calculated values by Fresnel reflection. The maximum off-axis transmission was 77% and the minimum transmission, at normal incidence, was 65% after surface reflection compensation, compared to the design values of 98% and 74%. Considering the maximum transmission angle that is matched with the design value within a degree, the thickness control of the middle layer was acceptable. If the thickness is not on target within 3nm, the maximum transmission angle would have been significantly changed. Since the deposition thickness control that is monitored with quartz micro-balancer, was under 1nm that is better than required thickness control. The thickness variation of the outer layer also does not give this kind of transmission loss.

It is suspected that the loss of transmission came from the scattered light from the relatively thick middle layer. The technique and equipment used for this deposition was optimized under a 100nm thick film. Thus, a 2767nm thick film could have a inhomogeneity that can create scattering. However it was not verified.

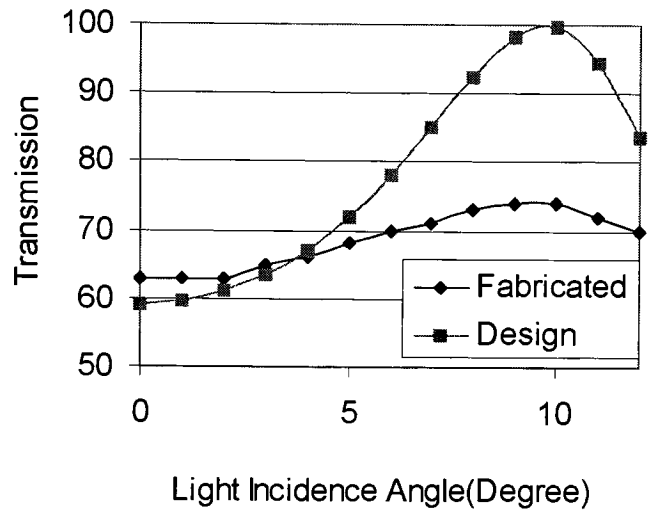


Figure 12. Transmission of fabricated filter

## 4.4. Lithography Results using Spatial Frequency Filters

Lithography was carried out with the ASML PAS 5500/300 stepper [76] with 0.5σ and 0.3 σ partial coherences, and a 0.63NA. The photoresist was UV110, by Shipley [77], coated to 0.42um thick on an organic antireflective film. Because the theory is based on coherent illumination, a 0.3 σ and the standard 0.5 σ were chosen for the experiment. Mask patterns were evaluated for isolated, semi-dense (1:5), and dense 250nm via-hole arrays. These conditions were not optimum for the fabricated filter, which was initially customized for 0.7NA and 180nm holes. For 250nm via-holes, higher attenuation is required. However, it requires more complicated manufacturing process.

In this study, the purpose of the imaging is to print smaller via-holes rather than print a specific size. When smaller sizes are possible, it is always possible to print bigger vias with a biased mask. Thus, it is not necessary to make the image size always the same as the mask size.

Minimum printable via-hole sizes were determined to have a 10% dose margin for 10% size variation. This means that the via-hole size is still remaining within 10% of minimum size while dose varies +/- 5% and a certain range of defocus. The defocus requirement, that is called depth of focus, varies with the exposure system and other process conditions. In this experiment, about 0.5μm was required. It is preferred to have a larger depth of focus for easier process control for the printing of the same size, or similar depth of focus for smaller sized patterns. It is also preferred to print but not necessary, via-holes that have similar sizes across density.

The reference group showed a big size difference between dense and isolated vias. Dense via-holes were printed at about 250 – 260nm, but isolated via-holes were about 210nm. The DOF was 0.4 – 0.6μm. Focus-Exposure plots for dense via-holes with 0.5 σ are compared in Figure 13 and one for 0.3σ is shown in Figure 14. Via-hole imaging with the filter produced very uniform results, as shown in Figure 15 and Figure 16. In all cases, the minimum via-hole sizes were 210nm – 220nm in the filtered image. The DOF was a similar level to that of the reference group. There was about 16% improvement in the dense via-hole and 4% for the isolated via-holes. The filtered results showed good resolution down to 210nm with reasonable focus and exposure margins. The reference

results are about 260nm with a 0.6um DOF. The filtered results, however, have a wider DOF than the reference results for bigger via-holes with a higher dose. The biggest merit of this filtered system was that the printed sizes of different densities were similar within 5% for smaller holes while the reference system showed about 15% difference.

Print holes with the filter were about 1.7 – 2 times more than the reference. The filter transmission was about 65% at normal incidence without surface reflection on the glass side. Glass reflects an additional 5%. The total loss at normal incidence is about 40%. Thus the dose difference is about order of tolerance.

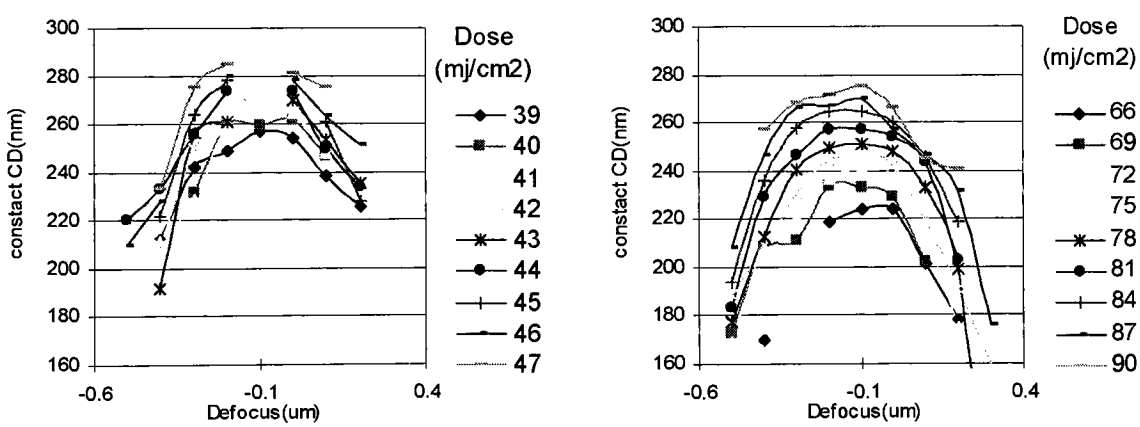


(a) Reference (b) Filtered

Figure 13. Dense 250nm via-holes with 0.5σ, 0.6NA.

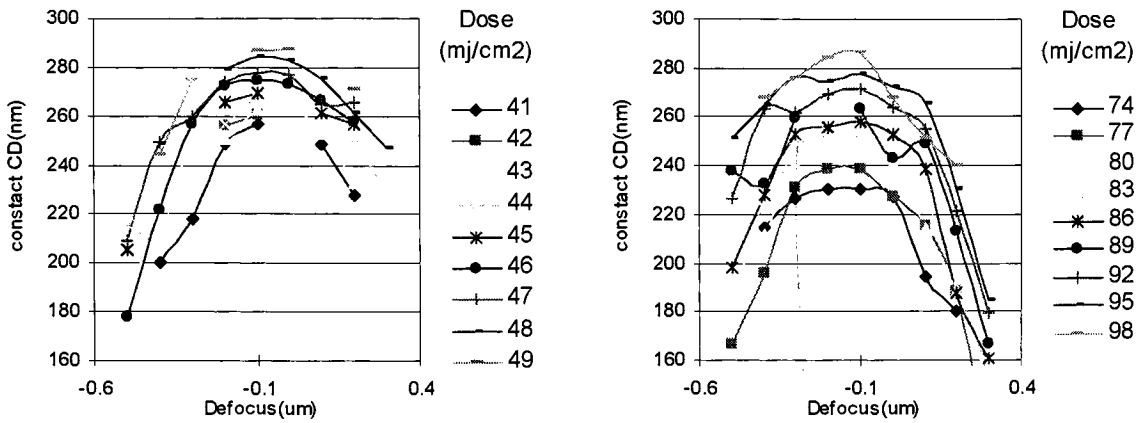


(a) Reference (b) Filtered

Figure 14. Dense 250nm via-holes with 0.3σ, 0.6NA

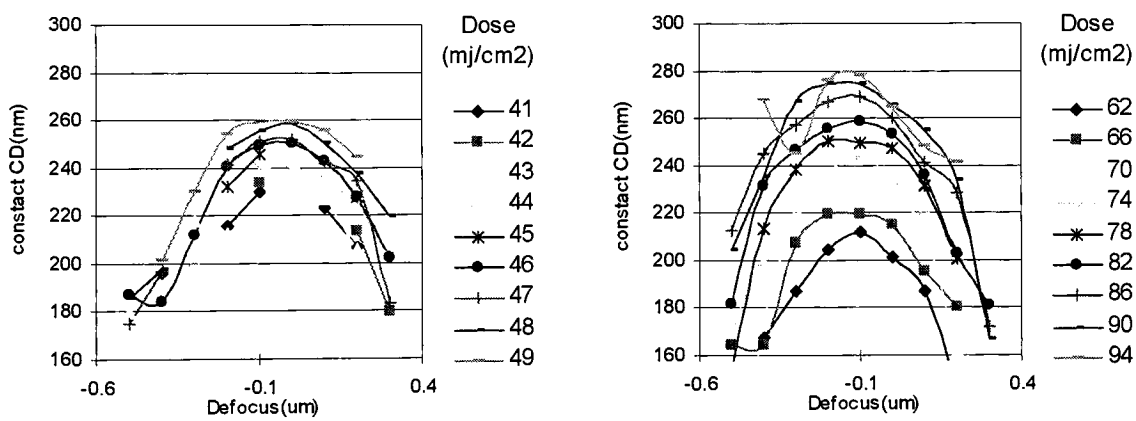


(a) Reference (b) Filtered

Figure 15. Semi dense 250nm via-hole with 0.3σ, 0.6NA

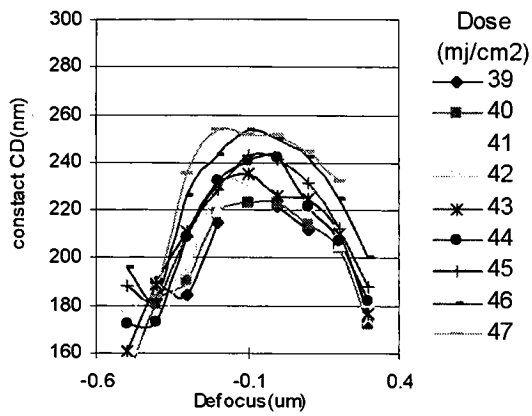


(a) Reference

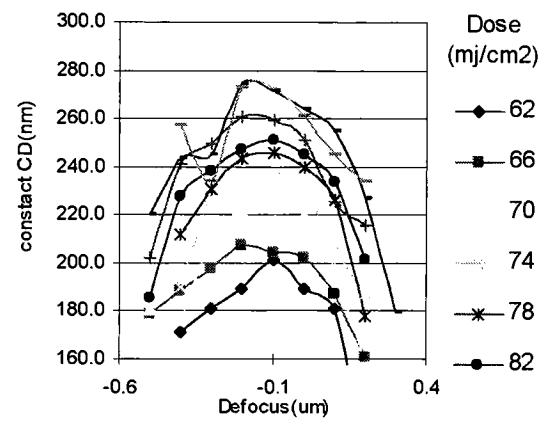


(b) Filtered

Figure 16. Isolated 250nm via-hole with 0.3σ, 0.6NA

Table 7. Lithographic results summary with and without spatial filter.

| Illumination | | Filtered | | | Reference | | |
|---|---|---|---|---|---|---|---|
| | | Isolated | Semi-iso | Dense | Isolated | Semi-iso | Dense |
| 0.3sigma | Size | 210nm | 215nm | 220nm | 220nm | 235nm | 260nm |
| | DOF | 0.5μm | 0.5 μm | 0.5 μm | 0.4 μm | 0.6 μm | 0.6 μm |
| 0.5sigma | Size | 210nm | 220nm | 220nm | 205nm | 220nm | 260nm |
| | DOF | 0.5 μm | 0.5 μm | 0.4 μm | 0.5 μm | 0.5 μm | 0.6 μm |

## 4.5 Spatial Filtering Conclusions and Future Work

Spatial filtering with an angular transmission filter was suggested and demonstrated as a new lithography technique. Multiple filter designs were successfully suggested and one of them was actually fabricated for lithography. The transmission results were not as designed. The fabrication process need to be refined, but showed good thickness control of the film. The lithography results showed up to 15% hole size reduction with different densities of via holes.

As numerical aperture increases, the peak transmission angle also increases. This will result in a thinner coating thickness, which makes the fabrication process easier. The fabrication process still needs to be fine tuned for better transmission. With better transmission and a better match with design, lithography is expected to print smaller geometries with a better process window.

# 5. Sub-Wavelength Optical Lithography Part 2: Lithography at 126nm

For the lithography below 157nm, several wavelengths has been investigated. Potential light source for suitable for lithography is considered and optical characteristics of those source have been explored also. Projection lens for the 126nm lithography evaluation tool has been evaluated and future improvement was investigated. Finally as imaging layer, silylation process has been evaluated.

## 5.1 Wavelength Considerations below 157nm

Optical lithography of below 157nm wavelength is very difficult. As well known almost all optical materials are not transparent at 157nm. Few exceptions are fluoride crystals as shown in Table 8 [78]. However, fluoride crystals in general have intrinsic birefringence. $CaF_2$ as main material for 157nm optics already has an unacceptable level of intrinsic birefringence that needs serious correction with combination of lens orientation. Other materials like $MgF_2$ have more birefringence than $CaF_2$, thus there are almost no acceptable optically transparent materials available below 157nm. For the window with no optical power, $MgF_2$ crystal can be used. $LiF_2$, another transparent candidate, is but hygroscopic and soft. So $LiF_2$ should be coated with $MgF_2$ to be used even after fabrication. These materials have very limited applications.

The projection optics should be a reflective system because there are no practical transparent materials below 157nm. Small part of the system can be refractive using $LiF_2$. Unlike refractive optics, reflective optics require large obscuration and/or strong aspheric

surface to make a high NA system [56]. Basic Schwarzschild lens design can be used for small field lithography such as direct write system as well as experimental lithography system. This study includes design and analysis of a high NA Schwarzschild lens.

Table 8. Properties of VUV transparent materials

| Material | Eg(eV) | Cut off waverlength(nm) |
|---|---|---|
| $BaF_2$ | 8.6 | 144 |
| $CaF_2$ | 9.9 | 126 |
| $MgF_2$ | 12.2 | 102 |
| LiF | 12.2 | 102 |
| NaF | 11.9 | 104 |
| $SiO_2$ | 9.6 | 130 |

Another problem of lithography with shorter wavelength below 157nm is the lack of a bright light source. For 436nm and 365nm, a mercury xenon lamp provides a stable and bright source with a narrow bandwidth. KrF, ArF, and $F_2$ excimer laser sources are very bright and have good characteristics at shorter wavelengths. There are a few candidates for wavelength shorter than 157nm [78]. One type is excimer lamp or laser. Another type is a Lyman source.

Lyman sources emit a radiation of 121nm, which is based on the atomic transition wavelength of hydrogen. So the bandwidth of the source is very narrow, which is required for any kind of refractive element with optical power. However, it is very

difficult to make a bright Lyman source. Total power of source is scalable but the area of source also will be increased.

The excimer lamp is the main interest to VUV lithography because it has the same wavelength with Argon excimer laser that can generate brighter light. Similar to excimer lasers, incoherent excimer sources generate photons in non-thermal gas discharges in rare gases or rare-gas halogen mixtures near atmospheric gas pressure. Typically, a dielectric barrier discharge ("silent discharge" or "ozonizer discharge") is applied. This discharge comprises of multiple self-pulsing microdischarges (lifetime of about 10 ns) that stochastically fill the discharge volume, resembling the plasma conditions of pulsed excimer lasers. Unlike lasers, these sources have a wide area of source plane, which makes it difficult to fit in the optical projection system. However it can be used for an experimental system with reduced source area. The typical radiant efficiency (electrical input power to radiant power) is about 10 percent, with a lamp lifetime of about 1000 hours.

There are some development efforts in Argon excimer lasers. They are still in the very primitive stage [79] - [82]. Because of the high energy requirement to activate Argon gas, it is required electron beam activation. There were several reports that states that an electron beam with near 700KV has high activation efficiency with 20atm argon gas and energy of pulse reached up to 40mJ/pulse and pulse width ranges from 5 to 20nsec. Development of such sources for optical lithography applications would be

feasible if the technology were beneficial. Thus argon excimer 126nm lithography was explored.

## 5.2 Projection Lens Evaluation for 126nm Lithography

At 126nm wavelength, a reflecting projection system is preferred because there are limited transparent materials. For a small field experimental system and small field applications, Schwarzschild lens can be used. The Schwarzschild lens has only 2 reflecting surfaces, thus it does not have chromatic aberration and has a very small aberration level for a simple design. Therefore a Schwarzschild reflective system can be used for a 126nm lithography test system.

A Schwarzschild system has no $3^{rd}$ order spherical, coma or astigmatism. Design of a system consists of two nearly concentric mirrors, hence there is only 3 degrees of freedom. Those are as calculated by Schwarzschild. For the infinite conjugate system, the design parameters follow those shown in Table 9 [83].

There are commercially available Schwarzschild microscope objective lenses. Among them, the Coherent model 25-2522 [84] has 36x magnification, 0.5NA, focal length 5.41mm, back focal length 8.6mm, and obscuration 12.2 % in area. This lens has about 0.5mm field of view. As a projection lens for 126nm lithography, this lens has been chosen and analyzed. Thus, the starting point of the design will have the dimensions as shown in Table 9.

The lens was optimized for 200μm field size diameter and 36 x magnification at 126nm. It was reverse engineered using GENII merit function, which is included in the OSLO lens design software [85]. Evaluation was carried out for all spherical surfaces of this commercial model and with one aspheric surface for future improvement. The optimized lens parameters are shown in Table 10 for both all spherical and single aspherical lens. The difference between the calculated and optimized parameter as shown in Table 9 and 10 respectively, is caused mainly by changing the conjugate parameter. The aspheric results are almost same as for all spherical designs.

Table 9. Basic parameter calculated with Schwarzschild equation and commercial lens.

| Parameter | | Equation | Commercial lens |
|---|---|---|---|
| Space between mirrors | d | $2fd = 2f$ | 10.82mm |
| Convex radius | R2 | $(\sqrt{5}-1)f$ | 6.6871mm |
| Concave radius | R1 | $(\sqrt{5}+1)f$ | 17.507mm |
| R1 to focus | | $(\sqrt{5}+2)f$ | 22.91mm |
| R1 clear aperture | | $(\sqrt{5}+2)y^2$ | NA |
| Fractional area osculation | | 1/5 | NA |

Optimization was mainly done to minimize wavefront aberration. However, ray intercept and other methods were also used to verify the viability of the design. For a short focal length with visible wavelength, Schwarzschild lens can have very low aberration at the center of field. This lens was evaluated for 126nm wavelength, which is

4-5 times shorter than visible wavelength. Thus wavefront aberration in unit of wavelength is 5 times larger than for the visible case that is original design target of commercial lens.

For an all-spherical design, in general the resulting aberration levels exceed the acceptable lithography levels. RMS OPD of lithography lens should be below 0.05λ. However, all spherical lens has 0.082 λ at the center of field, and 0.3 λ at the edge of field with perfect fabrication and alignment as shown in Table 12. Figure 18 and Figure 19 show wavefront aberrations for 0.28NA and 0.5NA Schwarzschild design.

Table 10. Schwarzschild lens optimized

| Parameter | All spherical optimized | Single aspheric optimized |
|---|---|---|
| Space between Mirror | 11.0584mm | 11.0584 mm |
| Convex radius | 6.773915 mm | 6.7959 mm |
| Concave radius | 17.7688 mm | 17.7603 mm |
| R1 to focus | 23.228 mm | 23.1719 mm |

Table 11. Optimized Aspheric parameter

| parameter | 4th | 6th | 8th | 10th |
|---|---|---|---|---|
| results | 1.5462e-8 | 1.711e-10 | -4.719e-14 | 5.84748e-15 |

Next the both lens design with all spherical and single aspherical mirror were evaluated for different conjugate where the lens can be used with small changes. As it goes higher in magnification, the aberration of the center of field improves but that of the edges of field degrades. This is caused by the optimization routine, which is a compromise between field points. At the center of field, high order spherical aberration was a major contributor to the RMS OPD error. Thus the aspheric surface would improve spherical aberration at the center of field. Major degradation at the field edge was caused by the field curvature as shown in Figure 18 and Figure 19 that show strong inward field curvature. Adding a very weak lens near the image plane to compensate for field curvature is recomended.

When the aspheric surface was introduced to a large concave mirror, the aberration at the field center reduced to $0.021\lambda$ which is deemed appropriate for lithography. However, the aberration at the field edge remained quite high. A major source of aberration is the field curvature, which is about one micron at the edge of field.

A similar trend of aberration and field curvature to the all-spherical lenses was observed with different conjugate. 38x magnification gives best performance at the center of field whose aberration is very similar with results optimization was done for center of field only.

The aspheric sag was calculated from the designed lens. Sag was 0.566 μm at the edge of lens as shown in Figure 17. Actually edge is raised, so center should be removed

for the fabrication process. Removal amount is about 1 wavelength with visible wave. This is well within measurement range for a conventional interferometer.

Tolerances for the Schwarzschild design are normally very tight. Curvature should remain within a wavelength of 126nm, which is normal production tolerance. Distance between the two mirrors is within a couple of micron and de-center of concave mirror should remain within 1 micron, which is a very tight tolerance.

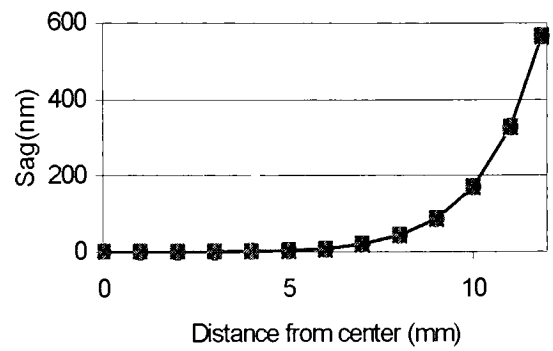


Figure 17. Aspheric departure of primary mirror

Table 12. RMS aberration with different conjugate with spherical and aspherical surface

| | All spherical | | | Single asphric | | |
|---|---|---|---|---|---|---|
| conjugate | Field center | 70μm | 100μm | Field center | 70μm | 100μm |
| 35x | 0.09135 λ | 0.1791 λ | 0.2876 λ | 0.04207 λ | 0.1057 λ | 0.2274 λ |
| 36x | 0.08164 λ | 0.1844 λ | 0.2964 λ | 0.02121 λ | 0.112 λ | 0.2356 λ |
| 37x | 0.07692 λ | 0.1912 λ | 0.3058 λ | 0.00339 λ | 0.1267 λ | 0.2508 λ |
| 38x | 0.07716 λ | 0.1991 λ | 0.3156 λ | 0.02351 λ | 0.1397 λ | 0.2633 λ |
| Optimized only for center | | | | 0.00248 λ | 0.125 λ | 0.2511 λ |

Table 13. Summary of tolerance in terms of wavefront aberration

(Peak to valley/RMS value)

| Tolerance parameter | Tolerance | On axis | 70μm | 100μm |
|---|---|---|---|---|
| Reference(optimized for center) | | 0.0708/0.0211 | 0.469/0.112 | 0.9136/0.2356 |
| Convex | 2 fringe(126nm) | 0.1175/0.0342 | 0.4483/0.1087 | 0.8892/0.2311 |
| Concave | 2 fringe(126nm) | 0.0851/0.0242 | 0.4683/0.1127 | 0.9118/0.2361 |
| Distance | 5 μm | 0.1598/0.0478 | 0.6236/0.1566 | 1.084 /0.2794 |
| De-center convex | 0.1mm | 0.0724/0.0211 | 0.4701/0.1121 | 0.9147/0.2358 |
| De-center Concave | 1μm | 0.3389/0.7123 | 0.653/0.1313 | 1.089/0.2455 |

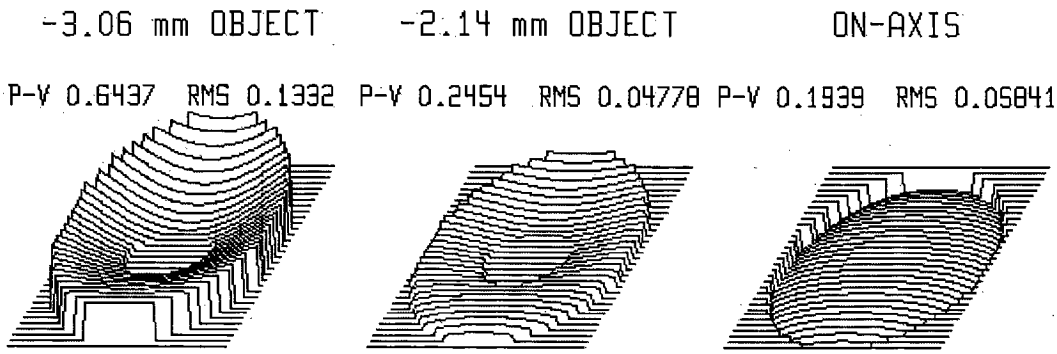


Figure 18. Wavefront aberration of 0.28NA Lens

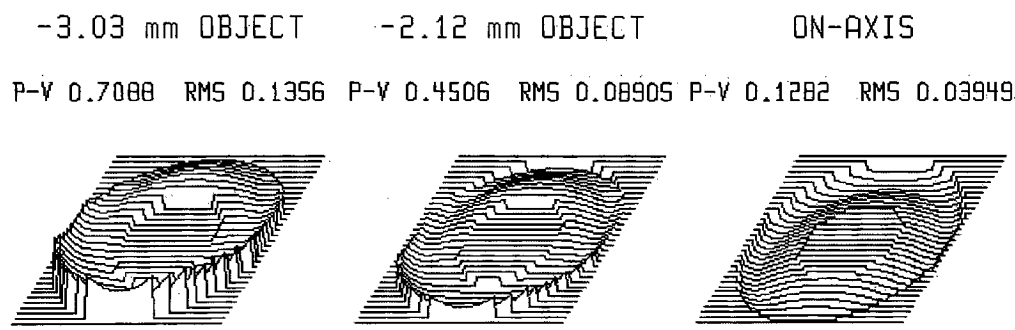


Figure 19. Wavefront aberration of 0.5NA lens with aspheric surfaces

## 5.3 126nm Lithography System Design

A small field experimental 126nm projection lithography system was designed [86] based on the commercial Schwarzschild lens for this experiment. For the illumination system consisted of a simple single spherical mirror with a slight tilt. The magnification of projection system is 15x and the maximum numerical aperture of illumination optics is 0.019.

With the 0.28NA projection system, depth of focus is about 1.6μm. Thus fine focus control is still required for the imaging. A capacitance gauge, ADE technologies's module 3800 and a passive gauge 2810 [88], were installed between the projection lens and the wafer for finer focus control. This setup can deliver a focus resolution to the level of 1nm depending on the set up, however the actual number can vary with wafer condition and conduction of ground path. A granite wafer chuck coated with chrome was used to make a conductive path for the capacitance gauge. In this system, the readout precision was limited to 0.07μm, which is about 5% of total focus budget for maximum resolution. The capacitance gauge itself has a much higher precision, however output precision is limited by the readout device.

Similar to 157nm and 193nm, 126nm can generate ozone in the light path that can block the light. Thus, the light path should be purged with clean nitrogen free from oxygen and water vapor. All optics were enclosed in a sealed box purged with clean nitrogen as shown in Figure 20 and Figure 21.

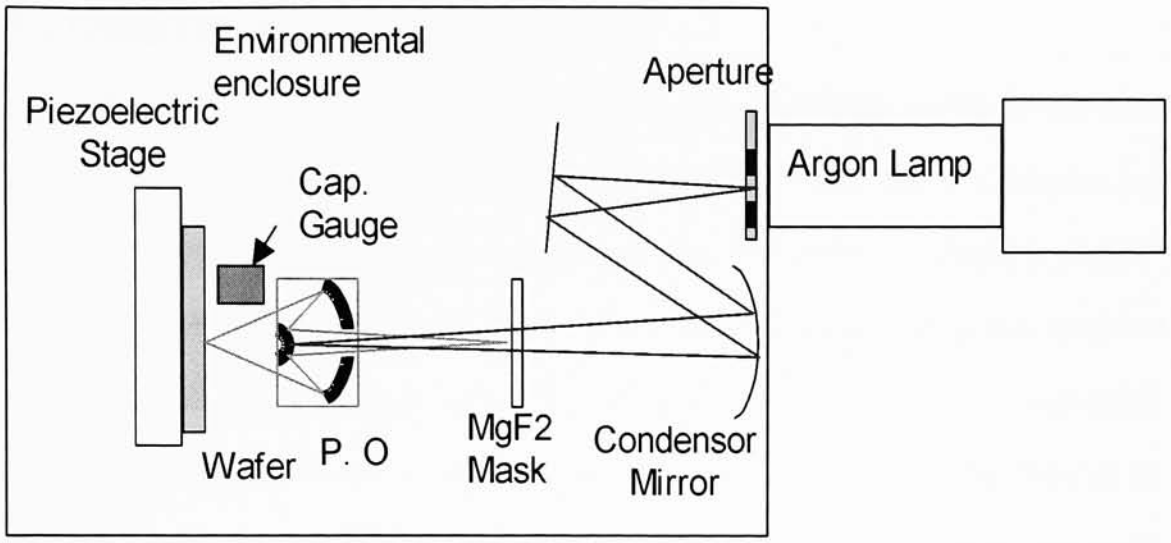


Figure 20. Exposure system enclosure diagram.

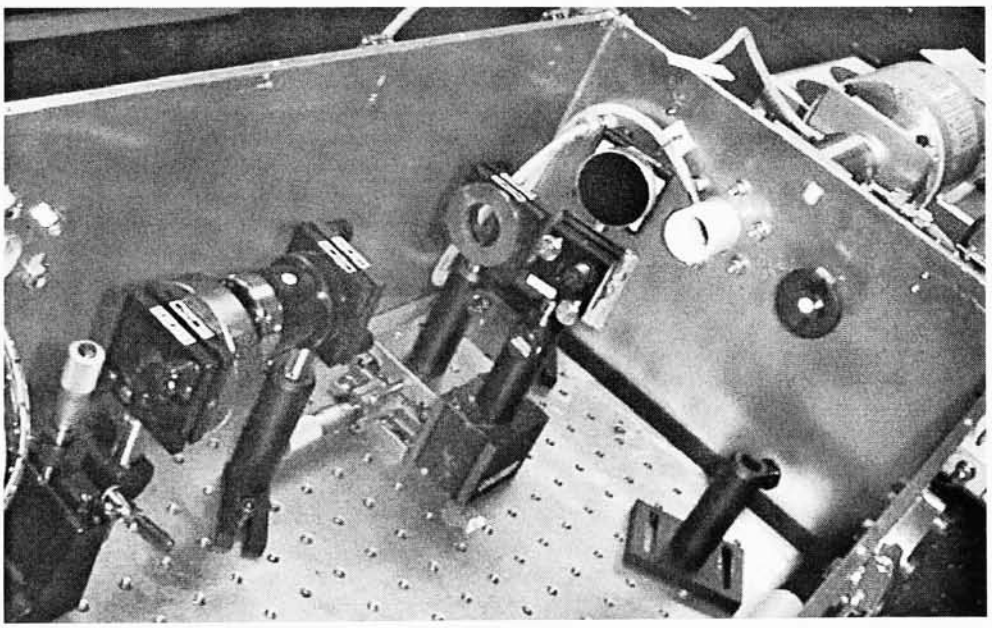

Figure 21. Assembled exposure system (Top cover is opened for display)

## 5.4 126nm Lithography Resist Processes

To date, no organic polymer transparent to the wavelength of 126nm has been reported. Due to the high absorption, surfaces to a depth of a few tens of nanometer can be exposed at 126nm. Thus, surface imaging or ultra thin resist is possible at 126nm. Traditional silylation [89] process was applied with DUV negative amplified resist to have surface imaging. Shipley DUV resist SNR248 was used with 110°C soft bake, 120°C PEB with about 400nm thickness. Reasonable selectivity could be obtained at 1mJ/cm$^2$ exposure as shown in Figure 22. For temperatures above 58°C, there was small amount of silylation in exposed area. However at this temperature the unexposed area was already silylated completely down to bottom of resist. The optimum temperature was 58°C, considering the required silylation thickness for dry development.

Under these conditions, the initial results using via-hole printing showed a promising possibility. Exposure was about 0.5 - 1mJ/cm2 was estimated from the lamp manufacturer's data. Silylation condition was 10torr with Di-Methly Silazane Di-Methyl Amine(DMSDMA), 60°C, 4min in the vacuum oven. With making a rough contact printing with $MgF_2$ mask, 3um line and spaces image were produced, which were the smallest features available on the mask.

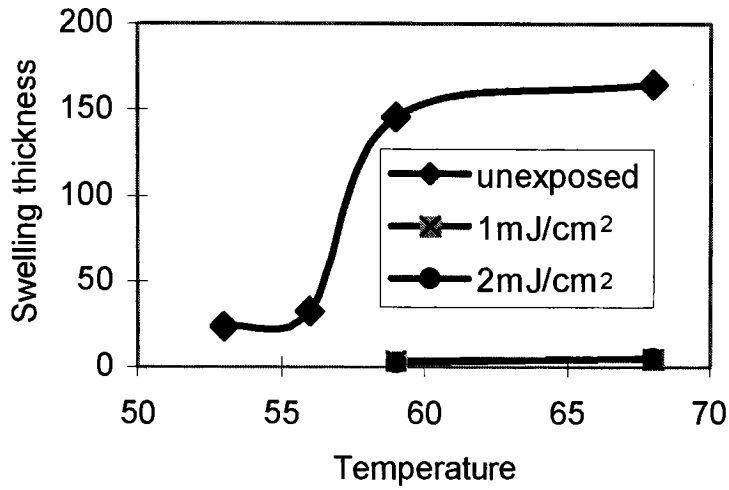


Figure 22. Silylation selectivity

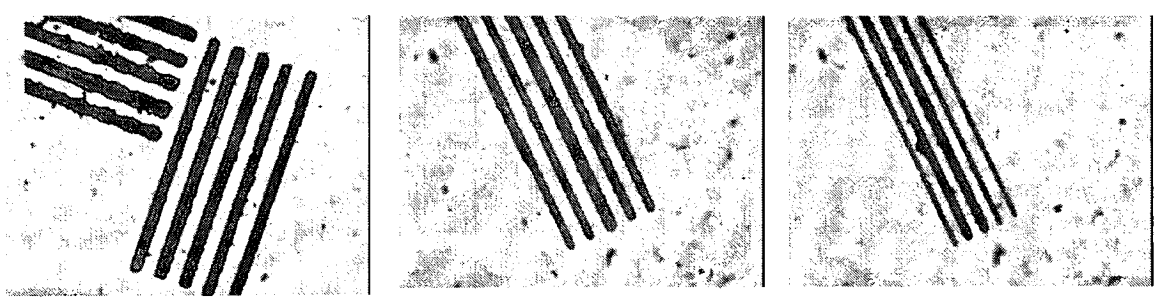

(a) 5 μm Line/Space (b) 4 μm Line/Space (c) 3μm Line/Space

Figure 23. 126nm silylation images using contact printing

## 5.5 126nm Lithography Conclusions

Schwarzschild objective lens designs were evaluated for 0.28 and 0.5NA. Both lens required an aspheric surface to meet aberration requirement within a small field. Higher numerical aperture would require multiple refractive elements, however there are no functional materials available at this wavelength. Thus 0.5NA is the maximum numerical aperture for this lens design.

A prototype experimental exposure system for 126nm lithography is developed with 0.28NA Schwarzschild optics. A simple Schwarzschild system can have good imaging quality for experimental purpose. Resolution of this system is expected to be as small as to 0.2um.

With a proper selection of organic or inorganic surface imaging techniques, sub-quarter micron resolution is expected. Silylation process responds well to 126nm illumination. It is expected to be a promising for the experiment as well as manufacturing processes.

With cryogenic liquid immersion, numerical aperture of an all refractive projection system can reach about 0.7NA. However this NA is not enough to compete with liquid immersion 193nm lithography. Thus, effort was concentrated on 193nm immersion lithography.

# 6. Sub-Wavelength Optical Lithography Part 3: Liquid Immersion Lithography

As an alternative to 126nm immersion lithography, initially water immersion lithography at longer wavelength was suggested. As comparable candidate to liquid argon, water was chosen as immersion medium. Ultimate resolution of 193nm water immersion should be comparable or better than 126nm lithography since water is transparent to 193nm and have higher index than visible wavelength. Optical requirements of immersion liquid have been explored for various aspects. Interferometric lithography system was designed and built for 193nm excimer layer and lithography for the below 50nm resolution was explored.

## 6.1 Optical Characteristics and Requirements of Immersion Fluids

The effect of dispersion of a liquid can be calculated as outlined below. The optical path length for a liquid with thickness $t$ and index $n$ is simply $tn$ for paraxial optics. Optical path difference caused by small index change should be much smaller than $\lambda/4$ to avoid chromatic aberration. However, the estimate changes for higher NA optics such as NA >1.0, because the paraxial approximation fails. To have minimal chromatic aberration, $\delta n$ should be smaller than Equation (21). This calculation will work for all kinds of index variations including chromatic aberrations and thermal index variations.

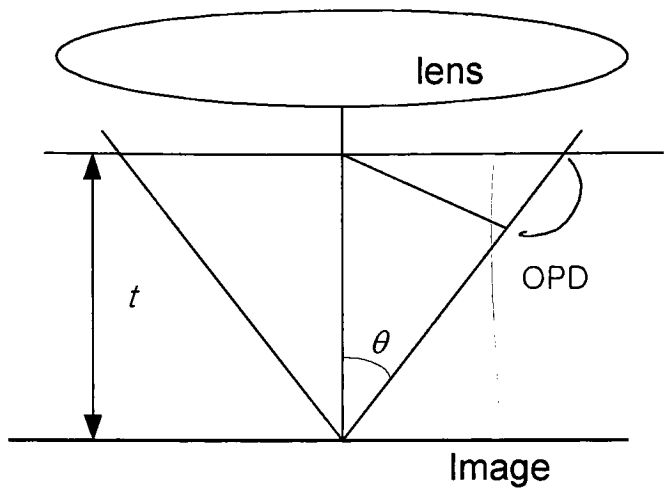


Figure 24. Optical path difference caused by liquid or defocus

Figure 24 displays the optical path difference in an imaging system with index variation. When an image is formed with index n, the phase difference between the normal incidence and oblique incidence at the top of medium with thickness t is described in Equation (18) :

$$Phase = \frac{2\pi nt}{\lambda}\left(\frac{1}{\cos\theta} - 1\right) \tag{18}$$

The phase difference caused by a uniform index change $\delta n$ should be smaller than Rayleigh's quarter wave criteria to make a good image. In actual lithography systems, phase differences should be much smaller than a quarter wave length to have good process margin.

$$Phase\ difference = \frac{2\pi\delta nt}{\lambda}\left(\frac{1}{\cos\theta} - 1\right) \tag{19}$$

$$\delta nt(\frac{1}{\cos\theta}-1)\leq\frac{\lambda}{4} \tag{20}$$

Thus the required index variation limitation is.

$$\delta n\leq\frac{\lambda}{4t}\frac{\cos\theta}{1-\cos\theta} \tag{21}$$

When index is fluctuated for any reason within a local area, the maximum allowable index change should be much smaller than Equation (21). The maximum allowable local index fluctuation is given Equation (22) and (23).

$$\frac{\delta nt}{\cos\theta}\leq\frac{\lambda}{4} \tag{22}$$

$$\delta n\leq\frac{\lambda\cos\theta}{4t} \tag{23}$$

These index variation criteria includes color dispersion and index change by temperature and pressure.

Table 14. $\delta n$ requirement at 193nm in ppm by Equation (21) for global index change

| NA | | 0.7 | 0.8 | 0.9 | 1 | 1.1 | 1.2 |
|---|---|---|---|---|---|---|---|
| Working distance (mm) | 10 | 35 | 25 | 18 | 13 | 9 | 6 |
| | 5 | 69 | 50 | 36 | 26 | 19 | 13 |
| | 1 | 347 | 248 | 180 | 130 | 93 | 64 |

Table 15. $\delta n$ requirement at 193nm in ppm by Equation (23) for local index non uniformity.

| NA | | 0.7 | 0.8 | 0.9 | 1 | 1.1 | 1.2 |
|---|---|---|---|---|---|---|---|
| Working distance (mm) | 10 | 4 | 4 | 4 | 4 | 3 | 3 |
| | 5 | 8 | 8 | 8 | 7 | 6 | 6 |
| | 1 | 42 | 40 | 38 | 35 | 32 | 28 |

In the Table 14 and Table 15, the index variation requirement is summarized with various assumptions. Water [64] is a perfect candidate as an immersion liquid for 193nm lithography. Transmittance of 1cm thick pure water is about 90%. Index of water at 193nm is 1.436 that is high enough to meet merit of immersion lithography as shown in Figure 25. According to previous research, water index changes less than 100ppm per 1°C at room temperature and 2ppm per 1pm wavelength change. Refractive index changes by 0.4 – 0.6ppm considering the laser wavelength bandwidth about 0.2 – 0.3pm. When water temperature is controlled under 0.1°C at room temperature, NA can be higher than 1.0 with reasonable working distance of 1mm or below.

A liquid for immersion lithography should be very transparent. Otherwise, it can absorb light. Transmission of water was measured with spectrophotometer. Fused silica cells with two different thicknesses of 15 mm and 30 mm were used for calibrating the surface effect. Cell windows have to be cleaned very carefully for almost 100% transmission for 193nm except Fresnel reflection. After cleaning with solvent, oxygen plasma was applied to remove residual solvent and organic residues. After cleaning, both

cells showed about 81% transmission without water. Loss of transmission was caused by the surface Fresnel reflection. To measure pure water transmission, transmission from 30mm cell was divided with 15mm cell to compensate for all surface reflection and transmission loss caused by test cell.

According to the transmission measurement as shown in Figure 27, higher temperature gives slightly lower transmission and the absorption edge shift to a longer wavelength. Lower temperature gives better transmission and smaller index change with temperature. This gives a reason to change lithography system temperature below 20°C in addition to lowering the dn/dT.

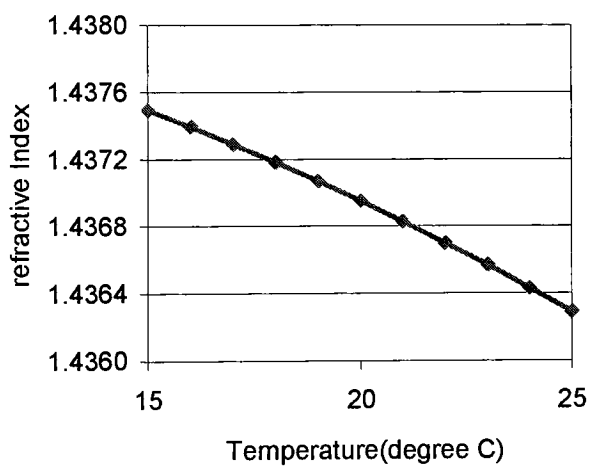


Figure 25. Refractive index variation with temperature

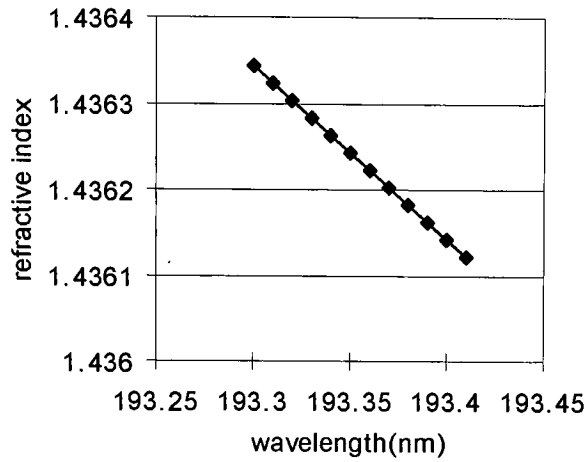


Figure 26. Refractive index variations with wavelength

In the semiconductor manufacturing facility, the immersion water can be contaminated with solvent or chemicals. However, keeping the contamination below 10ppm-100ppm does not cause serious transmission losses. The contamination level of the most abundant solvent in the semiconductor manufacturing facility, Isopropyl Alcohol (IPA) can be allowed up to 1000ppm. In Figure 28, the contaminated water transmission with common resist solvent, IPA and acetic acid is displayed. The small amount of acetic acid in the immersion water, can also be used to prevent T-topping resist.

Because of very high NA, low transmission can cause unbalanced absorption over pupil. In general, absorption at the center of pupil is preferred for high pass filtering. However, the edge of pupil always has higher absorption. When NA is 1.1, distance ratio between normal incidence and maximum angle of incidence is $\cos(\sin^{-1}(1.1/n)=1.55$. Transmission ratio is $10^{-\alpha t*0.55}$ is amount of apodization effect. If not, the transmission

loss at the edge of pupil will create an apodization that creates contrast loss and other problems in the image. If we want to keep the ratio less than 2%, $\alpha t$ should be less than 0.016. Considering the absorbance of water of about 0.05, thickness of water should be less than 3mm.

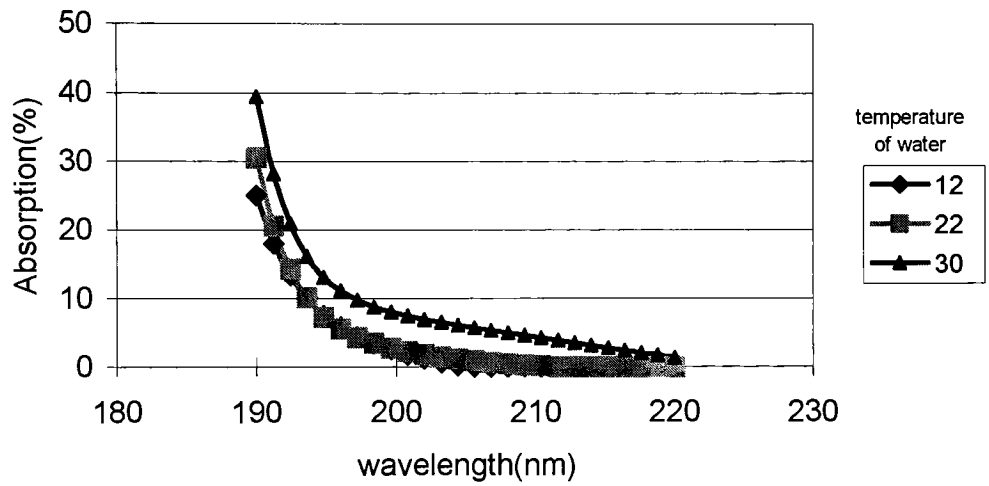


Figure 27. Absorption of 1cm water down to 190nm

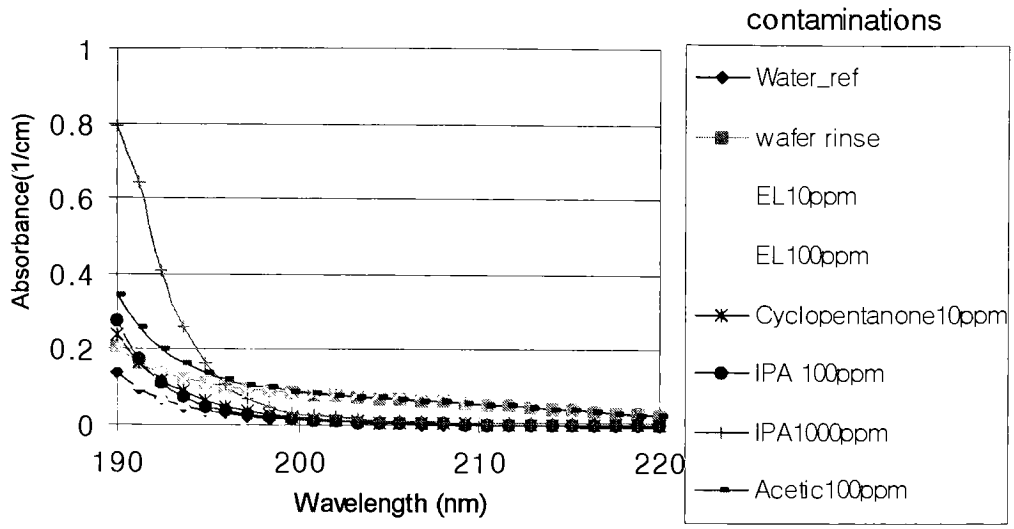


Figure 28. Absorbance of contaminated water

## 6.2 Interactions between Immersion Liquid and Photoresist

Photoresist used in the lithography is very sensitive to contamination. Chemically amplified resists are more sensitive than other types of resists. In the initial introduction of chemically amplified resists, chemical contamination was a serious problem. Chemically amplified resists are susceptible to process conditions and airborne contamination. Underlying substrates also influence the resist profile. Most of positive chemically amplified resists suffer from the formation of an insoluble layer or T-top profile depending on the contamination level. This is caused by the absorption of base materials from the air. Major base sources are HMDS, N-methylpyrrolidone and base material from the wall paint.

To solve the T-top problem, several methods have been suggested and evaluated. Those methods are adding base additive, supplying acidic material before development and modifying the polymer properties. Significantly lowering or raising de-protection energy of polymer can reduce the T-top problem. Lowering the de-protection energy [90] makes less time to have contamination reaction the by de-protecting polymer just with exposure before PEB. Raising de-protection energy [91] makes possible very high temperature bakes such that no base can be absorbed in the resist.

In water immersion lithography, water can be absorbed in the resist then behave as an acid consuming medium or acid generator can be leached out to water. Cure for this problem can be similar to the cure for the T-top problem. Solutions can be : (a) more hydrophobic surface, (b) denser material, and (c) added acid on top of resist.

Interaction between resist and water can be tested by immersion in water after dry exposure. For the test a matured DUV resists and i-line resists are better than immature 193nm resist. Easiest metrics are contrast and sensitivity. When acid generator diffuses to water from chemically amplified resist, sensitivity will be lower and contrast in general will be higher. Thus it is possible to find amount of reaction and correction requirement for the immersion exposure.

OCG OIR620 [92] Novolac resist for i-line system was used for verification purpose. Soft bake temperature was 110°C and PEB was 120°C. With this condition, negligible water-resist interaction is expected. Water rinse before develop was 60 seconds, which is relatively long enough for the immersion lithography. For each condition, 2

wafers were tested. Figure 29 shows contrast curves for silicon substrate and Figure 30 shows contrast curves for resist on an antireflective coated silicon substrate. Immersed wafers were expected to show a slower photo speed. However it was very difficult to find the difference between immersion and the reference group.

Figure 31 shows the process window comparison results for a chemically amplified resist. TOK DP 7126 [93] was tested with and without water immersion similar to the novolac resists case. A 150nm via-hole printing shows little difference between immersion and dry lithography. For small dose and defocus, immersion shows a rapid reduction of size. In the case of nominal dose for 150nm case, no differences between immersion and dry lithography were observed. Reduced sizes of via-holes were from the surface inhibition layer caused by immersion water. This problem can be reduced with minor modification in the resist.

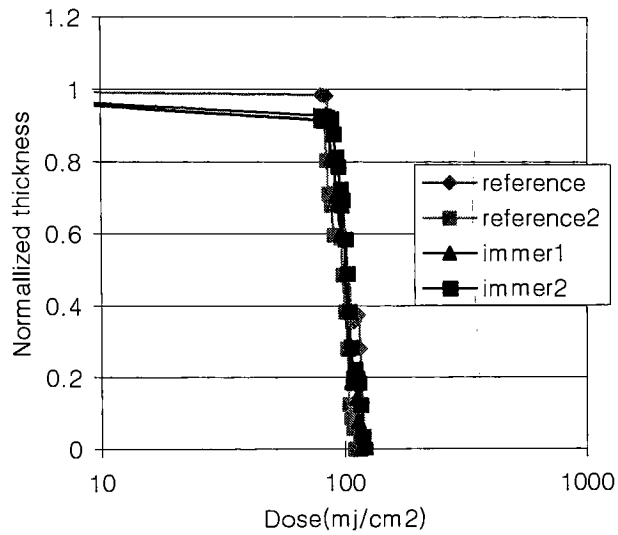


Figure 29. Comparison of contrast curve with immersion with novolac resist OIR620 on silicon

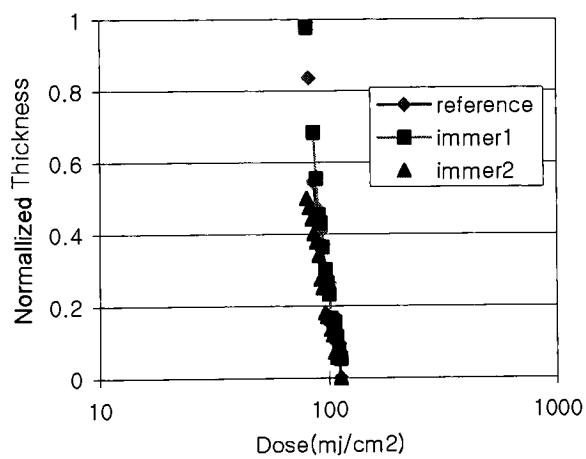


Figure 30. Comparison of contrast curve with immersion with novolac resist OIR620 on organic ARC

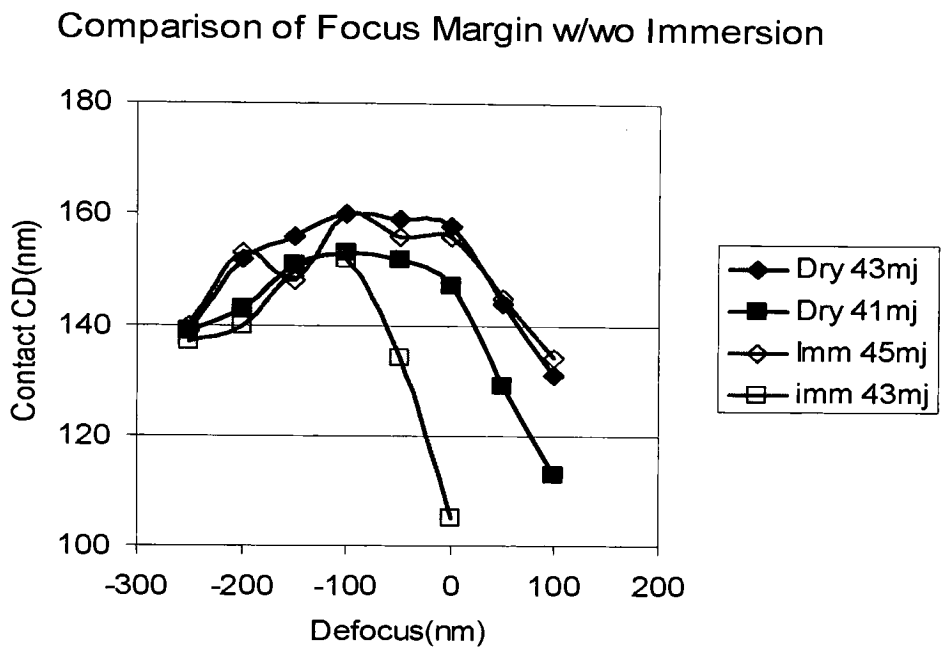


Figure 31. Comparison of process window of via-hole pattern dry and immersion imaging with chemically amplified resist TOK DP7126

## 6.3. Image Contrast Estimation for Lithography

Estimation of image contrast in lithography can be simplified with the contrast of 2-beam and 3-beam interference. When light waves propagate and interfere with each other in the resist, there are several factors that affect contrast. Different polarization can have different transmissions through the surface. The interference for the TM polarization is proportional to the cosine of the angle between incident beams. Also, when the beam is

diffracted at the mask or grating, there are different intensities for the different order of beams with different angles of diffraction.

Diffraction angle and intensities can be calculated using a Fourier transform with small amount of radiometric correction for the larger angle diffraction. In a general lithography case, radiometric correction factor is less than 2 -3% because of demagnification of the mask image. Fresnel electric field vector transmission coefficient are given in Equation s (24) and(25).

$$t_{TE} = \frac{2\sin\theta_t \cos\theta_i}{\sin(\theta_t + \theta_i)} \tag{24}$$

$$t_{TM} = \frac{2\sin\theta_t \cos\theta_i}{\sin(\theta_t + \theta_i)\cos(\theta_i - \theta_t)} \tag{25}$$

Vector interference [94] -[101] contrast in the resist with TE polarization is unity for all angles. However, in the case of TM polarization, image contrast is proportional to the cosine of incidence angle of the 2 beams.

In the case of equal angle 2-beam interference lithography, the contrast is simply the inner product of two vectors. In the case of 3-beam interference, which is more like a real projection lithography, it is more complicated because it has different radiometric effect and transmission. When intensities of 2 beams are same, the contrast is given in Equation (26) and (27). When the intensity of center beam is same as the sum of 2 other beams in a 3 beam interference, as in the case of dense line and spaces, contrasts are

given in Equation (28) and (29) that include radiometric effect, Fresnel reflection, and transmissions.

$$Contrast(TE, 2beam) = 1 \tag{26}$$

$$Contrast(TM, 2beam) = \cos(2\theta_t) \tag{27}$$

$$Contrast(TE, 3beam) = \cos(\theta_t / M)\frac{2\sin\theta_t \cos\theta_i}{\sin(\theta_t + \theta_i)} \tag{28}$$

$$Contrast(TM, 3beam) = \cos(\theta_t / M)\cos(\theta_t)\frac{2\sin\theta_t \cos\theta_i}{\sin(\theta_t + \theta_i)\cos(\theta_i - \theta_t)} \tag{29}$$

Weighted average of contrast for TE and TM polarized light is plotted for 193nm dry, immersion, and 157nm dry imaging. For 2-beam interference, contrast of immersion lithography is slightly lower than that of dry imaging for the same NA as shown in Figure 32. This is caused by low contrast interference in TM polarized light. For very high resolution with strong dipole illumination, it is possible to use only TE polarized light. The contrast will always be near unity.

For 3-beam interference, immersion lithography has a much higher contrast than the dry imaging case, because TM contrast is relatively higher than 2-beam dry imaging and smaller Fresnel reflection makes higher contrast at high NA case with TE polarized light.

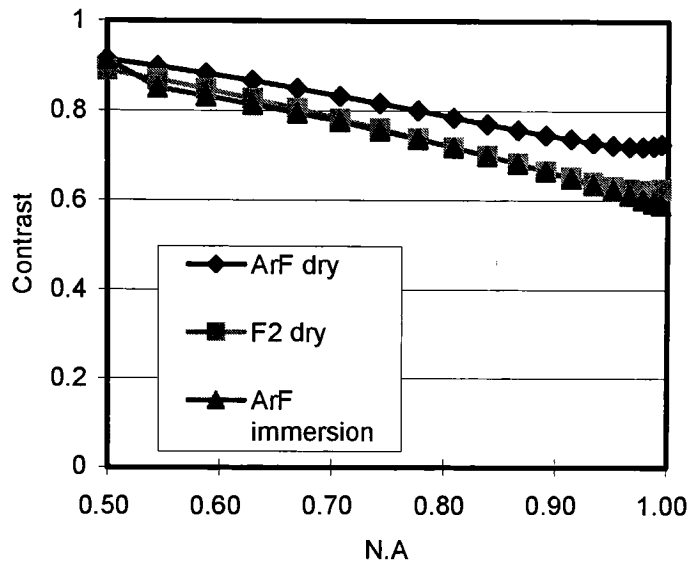


Figure 32. Two beam interference image contrasts with unpolarized illumination

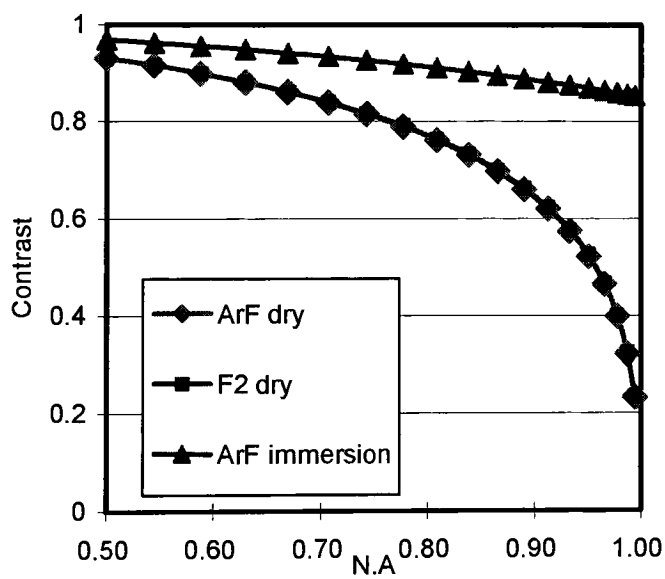


Figure 33. Three beam interference image contrasts with unpolarized illumination

## 6.4 Interference Lithography for Immersion Lithography Evaluation

Immersion lithography with real projection optics will require considerable resources and great deal of modification of the projection lens and stage system. Thus interference system [102] -[103] will be used for the evaluation of liquid immersion lithography. Interference lithography was previously evaluated for the experimental techniques or special application. In the Figure 34, the period of interference imaging is determined by the Equation (30).

$$\Lambda = \frac{\lambda}{2\ \sin(\theta)} \tag{30}$$

As shown in Figure 34, interference lithography system is very simple compared to the projection system. To introduce liquid in this system, only a matching optical index is required to keep incidence angle in the air preserved by the liquid. A prism can work for the matching optical index for a certain incidence angle. If it is required to change the angle of incidence, hemispherical lens is required.

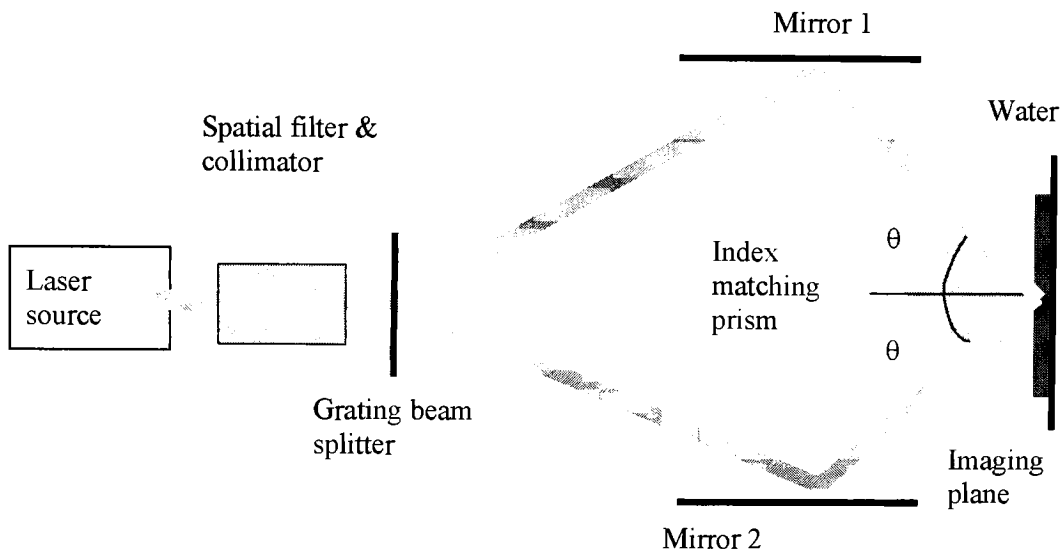


Figure 34. Diagram for simple interference lithography system

There are a lot of different setups for interference lithography. Some of the interesting designs are listed in the Figure 35. In general, the light source should be monochromatic. However, at the lithography wavelength, there are not many lasers with high coherence. Excimer laser can generate high power and short wavelengths but have broad spectral ranges and spatial incoherence.

Traditional interference imaging setup[97] is shown in Figure 35 (a). Type (a) uses a half mirror to split the wavefront. This setup is very simple, but the wavefront is mirrored and a laser source with very high spatial coherence is required. To solve this problem, type (b) has been suggested, but an additional mirror introduces complications in alignment and a longer path length. Type (c) has been tested by MIT Lincoln Lab. This

uses a Fresnel reflection by a thick silica plate. Still a very complicated beam path alignment is required.

As a different approach for a beam splitter, phase shift grating was introduced by MIT [100] as shown in Figure 35 (d). Phase shift grating can make multiple beams, but the first two have most of the energy. Using another grating, it can be converged to a point that creates interference imaging. Setup and alignment are very simple compared to other types. Because it uses 2 gratings, it is nearly achromatic. However this setup can make only one period pattern. When a different period is required, both gratings should be replaced. When a period relatively longer than the wavelength is required with a spatially coherent source, it is required to have a phase shift grating [101] as shown in Figure 35 (e). Two first order diffracted beams can interfere with each other and make interference pattern with a half period of the original grating. This is the simplest setup, but needs a very high spatial coherence to make a wider area.

The last type (f), a modified Talbot interferometer [103], consists of a simple grating beam splitter and 2 mirrors. The period of the interference image can be adjusted with mirrors. Wavefront orientation remains the same for both beams. Thus the spatial coherence requirement is relatively small. Also it has quasi-achromatic characteristics.

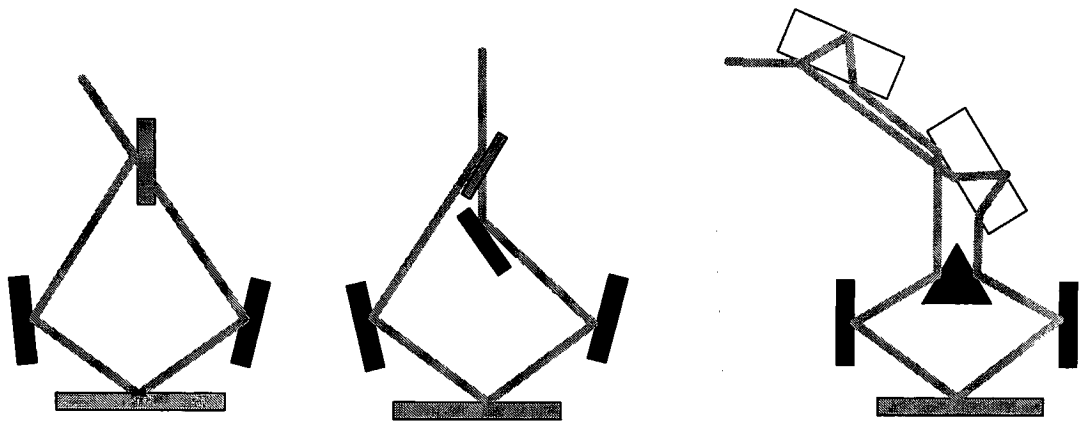

(a)IBM almaden (b) Half mirror with same orientation (c) MIT L.L type

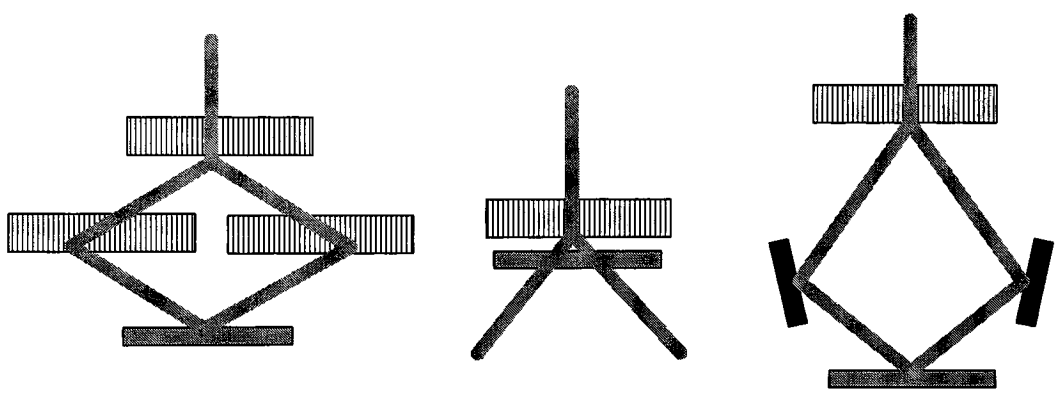

(d) MIT achromatic type (e) Bragg Grating (f) Grating Beam splitter

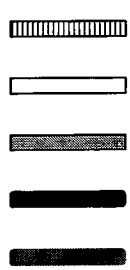

Grating

Glass with Brewster angle

Wafer -imaging plane

Mirror

Half Mirror

Figure 35. Various types of interference setup

When the laser is broadband, interference lithography gives narrow ranges of imaging because of beat frequencies of multiple wavelengths. In Figure 36, the period of the pattern is given by $Pw= \lambda /2\sin(\theta_w)$. For the fixed mirror type setups such as type (a), (b) and (c), $\theta_W$ is fixed and the period is only a function of wavelength. However in the type (d) and (f), $\theta_W$ is function of wavelength also. When laser source has different wavelength $\lambda_0$ and $\lambda_1$, in as the case of mirror beam splitter, the interference image has a beat frequency with period of

$$P_b = P(\lambda_0)\, P(\lambda_1) /(P(\lambda_0)- P(\lambda_1)) = 1/2\sin(\theta)*(\lambda_1*\lambda_0)/(\lambda_1-\lambda_0) \quad (31)$$

However in the grating beam splitter, $\theta_W$ is a function of wavelength because of the diffraction angle. The diffraction angle is $\theta_1 = \text{asin}(\lambda/P_g)$ where $p_g$ is the period of grating.

$$\theta_w = \theta_1 + 2\theta_2 \; \theta_W = \theta_1 + 2\theta_2 \quad (32)$$

$$P_w = \lambda/2\sin(\theta_w) = \lambda/2\sin\,(\text{asin}(\lambda/P_g + 2\theta_2) \quad (33)$$

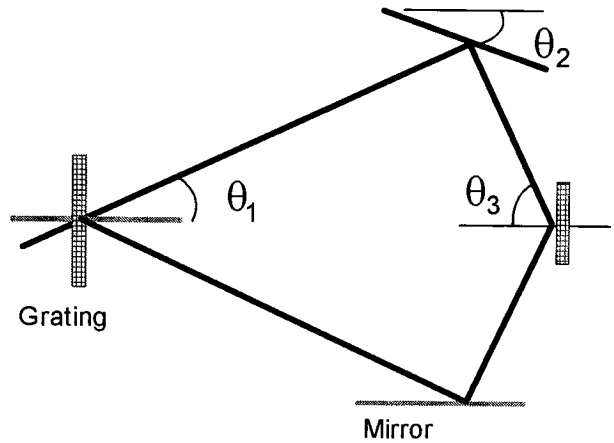


Figure 36. Quasi achromatic interference setup

When Pw = 2 Pg is desired, $\theta_2$ will be 0. Then, $P_w = \lambda/2\sin(\text{asin}(\lambda/P_g)) = 2P_g$. So this setup is completely achromatic. However when fabricating small period of grating, due to difficulty, reduction imaging is required. Then with $\theta_2 > 0$, it will not be complete achromatic will have achromatic characteristics. Beat frequencies at or near achromatic interference is calculated in Table 16

Table 16. Beat period with grating beam splitter.

| Bandwidth / Beam splitter | 10pm | 1pm |
|---|---|---|
| Grating period 1000nm | 5mm | 10mm |
| Grating period 600nm | 8mm | 80mm |
| Grating period 400nm | 150mm | 1500mm |
| Simple Half Mirror | 3mm | 30mm |

The bandwidth of illumination source can affect the image as described above. It also limits the path length mismatch between 2 paths in the interference setup. As well known, the coherence length is proportional to $\lambda^2 / \delta\lambda$. Temporal coherence length is about 4mm f or 10pm bandwidth that was used in this study setup. Thus the beam path length should be matched to within a millimeter to have good contrast. Spatial coherence will limit the tolerance of misalignment. For the 193nm beam, which is very difficult to align, it is required to have a few millimeters of spatial coherence. Excimer lasers used for lithography have only a few tens of microns of spatial coherence length. There were some efforts on developing a long spatial coherence excimer laser with a unstable resonator. Spatial coherence was enhanced to half millimeters recently. To achieve good uniformity in illumination, the laser beam will need to be expanded then the spatial coherence will also be magnified. With new spatially coherent excimer laser, it is now possible to make good interference images. The major specifications of excimer laser that was used for this research is Bragg star EX 10BM [105] as listed in Table 17.

Table 17. Specification of excimer laser for interference lithography

| | |
|---|---|
| Energy Control Range | 4-12 mJ |
| Repetition Rate | 100 Hz |
| Static Gas Life to 50% energy | 60 days |
| Pulse Length | 15 nS |
| Beam Size | 8 X 3-5 mm |
| Divergence | 1 X 2 mRad |
| Energy stability pulse to pulse | <2% Standard Deviation |
| Temporal coherence | 0.5mm –2mm |
| Spatial Coherence | >0.5mm for 193nm |
| Beam Uniformity | +/-5% |

## 6.5 Imaging Results with Interference Lithography

Initial lithography work was carried out with a multi mode 442nm He-Cd laser and a single mode 457nm Argon ion laser. The theoretical minimum period of a dry 442nm system is 221nm without immersion. In practice, however, it is about 310nm with 45° incidence. It is possible to increase the resolution with higher angle, but the gain is not so high due to difficulties associated with alignment and polarization issues. It is also not practical to have a higher angle in projection lithography. Thus, the interference lithography experiment was also done with up to 45° angle. In the case of immersion

interference lithography, the resolution can be improved by a factor of the index of a prism material when the immersion liquid has a comparable index at the low incidence angle.

In water immersion, the theoretical minimum period goes down to 165nm with a water index of 1.341 at 442nm. With a 45° setup, it is possible to print a 210nm pitch with glass prism. Figure 37 and Figure 38 show high resolution interference images with dry and immersion setups, respectively.

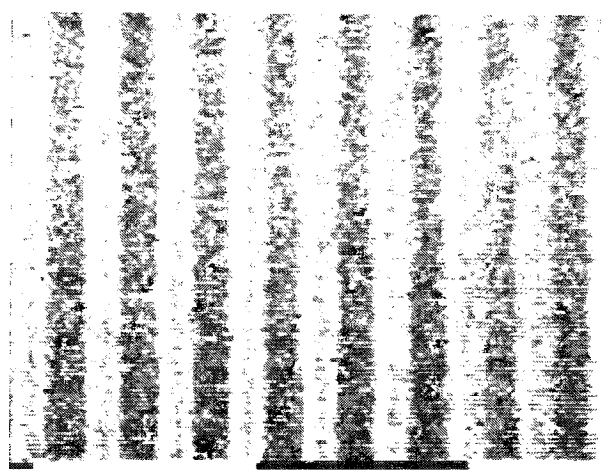

Figure 37. 320nm period images with dry interference lithography at 442nm with corresponding NA 0.74

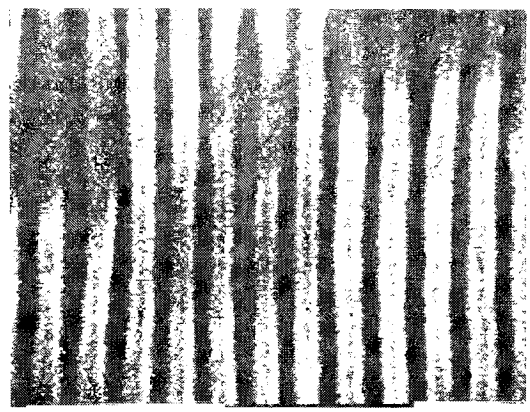

Figure 38. 230nm period images with water immersion interference lithography at 442nm withcorresponding NA 1.04

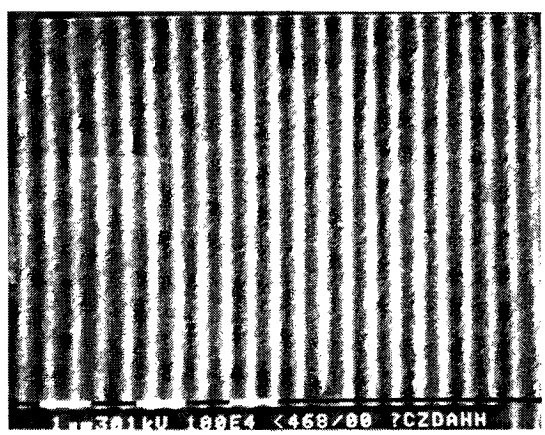

Figure 39. Clean interference image with coated optics

A minor problem was found during the experiment was found in immersion lithography. There are several surfaces in the beam path without an antireflective coating. Those surfaces generate lots of ghost images and parasitic interference as shown in Figure 38. Major sources of parasitic interference are reflection from the backsides of the index matching prism. With coated optics, it could be reduced as much as in Figure 39. In

a real projection imaging system, every surface has high transmission coating. Thus, the parasitic interference is not an issue.

The main target of this research is to make an immersion lithography image with 193nm that can practically extend optical lithography below 70nm resolution. As described in previous Section, it is difficult to make interference image because of the low temporal and spatial coherence nature of excimer lasers. Thus, the choice of excimer laser with high coherence was the key enabler for good interference. In addition to the laser, the interference beam path should be matched very well.

A system for immersion interference lithography has been built for proof of concept. An artistic diagram and actual picture are shown in Figure 40. Optical beam alignment was done carefully with He-Ne laser and Excimer laser.

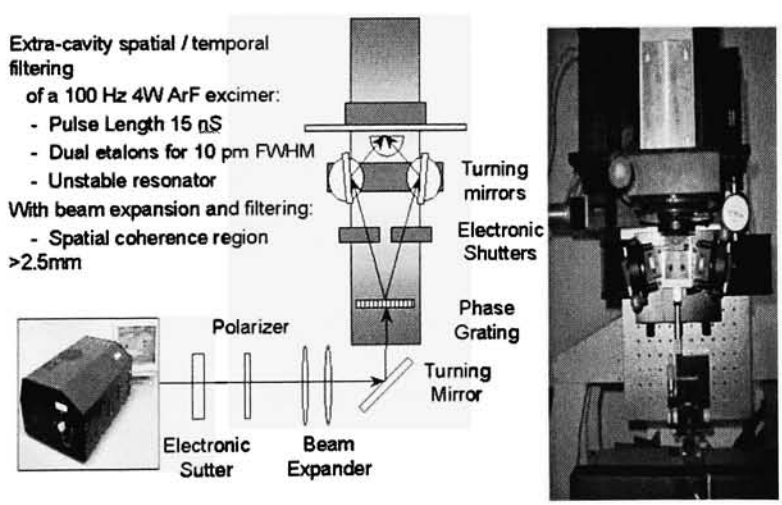


Figure 40. Immersion lithography system

Wafer was prepared with resist on antireflective coating to reduce interference effect due to resist thickness variation. Unlike longer wavelengh lithography, 193nm light interference is too severe to make good image because of high reflectance of silicon. Brewer Science ARC 29™ [106] was spun at 2600rpm resulting in 77nm thick coating and baked at 200°C. The photoresist used for this experiment was TOK ILP06™ which is an experimental immersion resist. It was coated at 4500 RPM resulting in a 72nm thick coating on antireflective layer coated wafer and followed by 115°C, 60sec bake to remove remaining solvent. The wafer was then exposed on the interference imaging system followed by PEB (post exposure bake) at 115°C 60sec to the chemical amplification and 30 second development with a tetra methyl ammonium hydride (TMAH) solution.

Because of very high resolution nature of immersion interference imaging, resist collapse and lifting are very serious problems. Solving pattern collapse or lifting is not part of this research. As an interim solution, the resist thickness was lowered to have low aspect ratio and a low viscosity rinse chemical 'OptiPattern™ Surface Conditioning Solution' by Air Products [107] was used after rinse before dry. Most critical part in this process was optical alignment of interference system and rinse to prevent collapse.

Using a dry imaging system with 30° incidence angle to the hemispherical lens in interference system with water, a 193nm pitch line and space pattern was resolved, as expected for the reference. Using the same system with water immersion, a 120nm pitch pattern was obtained, as shown in Figure 41. With higher angle 42° and 47° that have

corresponding NA of 0.8 and 0.96, 100nm and 90nm pitch patterns were resolved as shown in Figure 41 and Figure 42 respectively. Unlike argon ion laser and He-Cd laser interference with an excimer laser, the parasitic interference was not an issue because of the short coherence length. Instead of the parasitic interference, the alignment requirement was much tighter than in the He-Cd case. Higher angle corresponding to high numerical aperture images were also achieved. The highest NA that could create a good image was 1.05 and corresponding line and space size was 45nm as shown in Figure 41. As expected from the basic theory of interference and immersion lithography, the pattern pitch was well defined according to the incidence angle. With a higher angle and good alignment, it would be possible to print smaller features also.

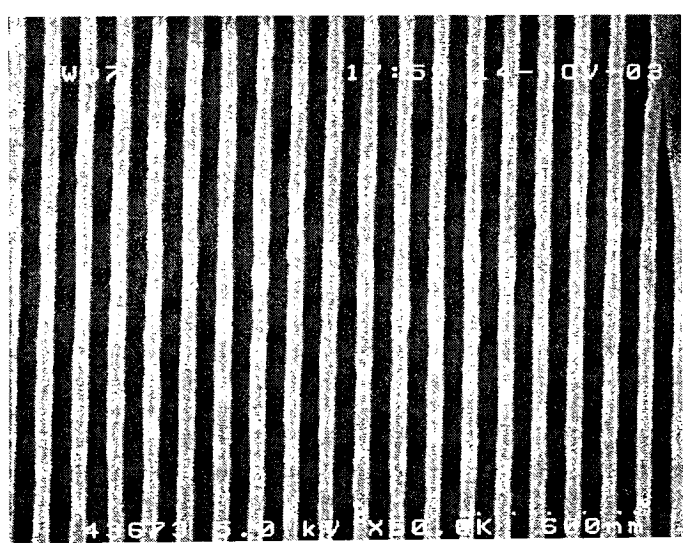

Figure 41. 120nm pitch pattern by 0.80NA Immersion imaging

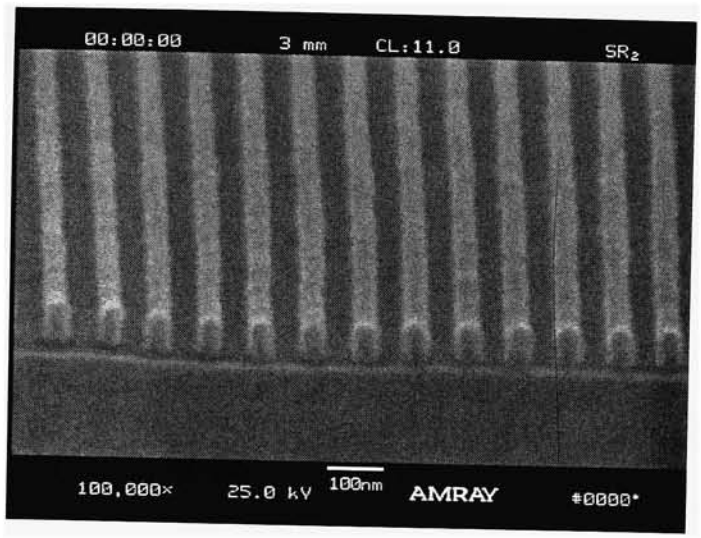


Figure 42. 90nm pitch pattern by 1.05NA immersion imaging.

## 6.6 Immersion Lithography Conclusions

Immersion lithography feasibility has been demonstrated for printing of features below 70nm with a 193nm wavelength. The temperature control requirement for controlling index variation is acceptable, with several millimeters working distance. Wavefront distortion or focus change can be minimized with tight temperature control. Image quality below 70nm with 193nm immersion can be adequate for those generations. TM polarization contrast became lower, whereas TE contrast remained the same or even higher with immersion lithography.

Finally, using interference techniques, 90nm pitch dense line and space were demonstrated with 193nm immersion lithography. With further improvement of the interference setup with a higher incidence angle, it can be expected to achieve print at about 35nm line and space resolution. An interference system can be used for immersion resist evaluation as a low cost substitute for a projection system. It also allows mimicking the low contrast image when using polarization control and zero order background light addition.

Immersion lithography is a very promising technology for extending current optical lithography to below 70nm and even further. Similar technology can be extended with shorter wavelengths, making even smaller geometries.

## 7. Sub-Wavelength Optical Lithography Conclusions and Summary

Optical lithography has been developing very rapidly for the last several decades. Every time it reached some limitation, a new technology was developed to extend its life. For numerous reasons, it was believed that with optical lithography with 70nm would be very difficult to achieve, and EUV or some other technology would take over.

In this research, extension of optical lithography is proposed and achieved. An alternative method of spatial filtering has been suggested and its performance was evaluated for via-hole imaging resulting in reductions of via-hole size by 15% or more. A 126nm lithography evaluation system was built and showed a simple imaging result with via-hole printing, except for projection imaging. Unfortunately, it turned out to be more practical to apply a shortened wavelength with liquid immersion lithography. Liquid immersion 193nm lithography, comparable to dry 134nm wavelength, is suggested and evaluated. The majority of problems that may be encountered in immersion lithography were evaluated and proven as acceptable or deemed a simple engineering problem. Interference lithography, which is a good means of proto typing and evaluating lithography, has been developed with an excimer laser at 193nm for the first time in the industry, using a modified unstable resonator excimer laser. Imaging results show line and space patterns below 50nm line and space beyond the 70nm lithography generations.

As a result of this study, the major contributions to lithography technology are listed in, but not limited to, the following.

A. An alternative method of spatial filtering in an angular dimension is introduced and successfully demonstrated.

B. Using the concept of spatial filtering and a novel approach in the imaging system, imaging of smaller via-hole is demonstrated, both with simulation and physical demonstration.

C. The potential of shorter wavelength lithography at 126nm was evaluated from the aspect of the photomask, imaging system, and resist processing components. It turned out to be more practical to use immersion lithography at 193nm rather than trying low NA (about 0.7) immersion lithography at 126nm.

D. Basic requirements in immersion lithography were evaluated as initial lithography development work, including index and transmission requirement calculation, measurements and evaluation of existing information, interaction between resist and water, and a study of performance with immersion lithography.

E. A new quasi achromatic interference lithography system using a 193nm excimer laser was developed, and imaging was demonstrated at a 90nm pitch for process evaluation.

For improvement in the future, the angular filter manufacturing process needs to be tuned for better performance. Immersion lithography still requires much study, including light scattering in a liquid medium, vector imaging effects, suppression of bubble generation from wafer handling, and resist-water interactions. There are more

issues that must be addressed in order for immersion lithography to be commercially available technology.

## 8. References


[1] The National Technology Roadmap for Semiconductors, Semiconductor Industry Association, San Jose, CA, 2002.

[2]. W. P. Ballard, D. A. Tichenor, D. J. O'Connell, L. J. Bernardez II, R. E. Lafon, R. J. Anderson, A. H. Leung, K. A. Williams, S. J. Haney, Y. E. Perras, K. L. Jefferson, T. L. Porter, D. Knight, P. K. Barr, J. L. Van de Vreugde, R. H. Campiotti, M. D. Zimmerman, T. A. Johnson, L. E. Klebanoff, P. A. Grunow, S. Graham, Jr., D. A. Buchenauer, W. C. Replogle, A. G. Smith, J. B. Wronosky, J. R. Dàrnold, K. L. Blaedel, H. N. Chapman, J. S. Taylor, L. C. Hale, G. E. Sommargren, E. M. Gullikson, P. P. Naulleau, K. A. Goldberg, S. H. Lee, H. Shields, R. J. St. Pierre, and S. Ponti, "System and Process Learning in a Full-Field, High-Power EUVL Alpha Tool," Proc. of SPIE vol.5037, 2003, pp.47-57.

[3] S. H. Lee, P. Naulleaub, C. Krautschika, M. Chandhoka, H. N. Chapmanc, D. J. O'Connelld, and M.Goldsteina, "Lithographic flare measurements of EUV full-field projection optics," Proc. of SPIE vol.5037, 2003, pp.103-111.

[4] S. P. Hau-Riege, A. Barty, P. B. Mirkarimi, D. G. Stearns, H. Chapman, D. Sweeney, M. Clift, E. Gullikson, and M. Yi, "Defect repair for extreme ultraviolet lithography (EUVL) mask blanks," Proc. of SPIE vol.5037, 2003, pp.331-338.

[5] J. Yamamoto, T. Iwasaki, M. Yamabe, N. Anazawa, S. Maruyama, and K. Tsuta, "EPL Stencil Mask Defect Inspection System Using a Transmission Electron Beam," Proc. of SPIE vol.5037, 2003, pp.531-537.

[6] H. C. Pfeiffer1, S. D. Golladay, M.S. Gordon, R. A. Kendall, J. E. Lieberman, J. D. Rockrohr, W. Stickel, T. Yamaguchi, K. Okamoto,T. Umemoto, H. Shimizu, S. Kojima, and M. Hamashima, "PREVAIL – Latest Electron Optics Results," Proc. of SPIE vol.4688, 2003, pp.535-546.

[7] M. Lercel, "Analysis of critical parameters for EPL mask fabrication," Proc. of SPIE vol.4688, 2003, pp.570-582.

[8] J. W. Strutt Lord Rayleigh, "Investigations in optics, with special reference to the spectroscope," Philosophical Magazine 8, 1879, pp. 261-274.

[9] J. W. Strutt Lord Rayleigh, "On the theory of optical instruments, with special reference to the microscope," Philosophical Magazine 42,1896, pp. 167-195.

[10] C.M. Sparrow, "On spectroscopic resolving power," The Astrophysical Journal 44, 1916, pp. 76-86.

[11] D. Nyyssonen Grimes, and B. J. Thompson, "Two-point resolution with partially coherent light," J. Opt. Soc. Am. 57,1967, pp. 1330-1334.

[12] B. J. Lin, "Where is the Lost Resolution?" Proc. of SPIE 633, 1986, pp. 44-50.

[13] H. H. Hopkins, "On the diffraction theory of optical images," Proc. Royal Soc of London, vol. 217A, 1953, pp.408-432.

[14] W. Arnold, and G. Escher, "Wafer steppers for 64M and 256M bit memory generations," CR #51, SPIE, 1993, pp. 42-81.

[15] C. Pierrat, F. Vinet, T. Mourier, and J. W. Thackeray, "ANR photoresist process optimization at 248 nm," Proc. of SPIE vol. 1262, 1990, pp. 301-311.

[16] C.G. Wilson, R.A. Dammel, and A. Reiser, "Photoresist materials : Historical perspective," Proc. of SPIE, vol.3049,1997, pp. 28-41.

[17] W. D. Hinsberg, S. A. MacDonald, N. J. Clecak, C. D. Snyder, and H. Ito, "Influence of polymer properties on airborne chemical contamination of chemically amplified resists," Proc. of SPIE vol. 1925, 1993, pp. 43-52.

[18] J. Moll and P. M. Schermerhorn, "Excimer laser induced absorption in fused silica," Proc. of SPIE. vol. 3679, 1999, pp. 1129-1136.

[19] V. Liebman, M. Rothchild, J.H.C. Sedlacek, R.S. Uttaro, A.K. Bates, and C.Van Peski, "Long term 193nm laser induced degradation of fused silica and calcium Fluoride," Proc. of SPIE. vol. 3679, 1999, pp. 1137- 1145.

[20] N. Kuzuu, "OH content dependence of ArF excimer laser induced absorption in type III fused silica," Proc. of SPIE. vol. 2714, 1994 pp. 71- 79.

[21] B. Wang, "Birefringence in fused silica and CaF2 for lithography," Solid State technology, vol. 43, No. 2, 2000, pp. 77- 82.

[22] J.H.C. Sedlacek and M. Rothchild, "Optical material for use with excimer laser," Proc. of SPIE. vol. 1835, 1992, pp. 80- 88.

[23] F. M. Houlihan, T. I. Wallow, A. G. Timko, E. Neria, R. S. Hutton, R. A. Cirelli, O. Nalamasu, and E. Reichmanis, "Recent advances in 193-nm single-layer photoresists based on alternating copolymers of cycloolefins," Proc. of SPIE vol. 3049, 1997, pp. 84-91.

[24] T. M. Bloomstein, M. Rothschild, R.R. Kunz, D.E. Hardy, and R.B. Goodman, "Critical Issues in 157nm lithography," J. Vac. Sci. technol.B. vol. 16, No. 6, 1998, pp. 3154- 3157.

[25] J. H. Burnett, R. Gupta, and U. Griesmann, "Absolute index of refraction and its temperature dependence of calcium fluoride, barium fluoride, and strontium fluoride near 157 nm," Proc. of SPIE vol. 4000, 2000, pp. 1503-1509.

[26] V. Liberman, M. Rothschild, N. N. Efremow, Jr., S. T. Palmacci, Jan H. Sedlacek, C. K. Van Peski, and K. J. Orvek, "Marathon evaluation of optical materials for 157-nm lithography," Proc. of SPIE vol. 4346, 2000, pp. 45-51.

[27] V. Liberman, M. Rothschild, J. H. Sedlacek, R. S. Uttaro, A. K. Bates, and K. J. Orvek, "Long-term testing of optical components for 157-nm lithography," Proc. of SPIE vol. 4000, 2000, p. 488-495.

[28] K. Mann, O. Apel, and E. Eva, "Chracterizing absorption and total scattering losses on optical components for 193nm wafer stepper," Proc. of SPIE. vol. 3679, 1999, pp. 1019- 1029.

[29] I. Toepke and D. Cope, "Improvements in crystal optics for excimer lasers," Proc. of SPIE. vol. 1835, 1992, pp. 89,-97.

[30] T. Onodera, T. Matsuo, T. Itani, and H. Morimoto, "Investigation of attenuated phase-shifting mask material for 157-nm lithography," Proc. of SPIE vol. 4346, 2001, pp. 61-71.

[31] R. H. French, J. S. Gordon, D.J. Jones, M. F. Lemon, R.C. Wheland, X. Zhang, F. C. Zumsteg, Jr., K. G. Sharp, and W. Qiu, "Materials design and development of fluoropolymers for use as pellicles in 157-nm photolithography," Proc. of SPIE vol. 4346, 2001, pp. 89-97.

[32] P. L. Reu, A. R. Mikkelson, M.P. Schlax, E. P. Cotte, L. K. Siewert, R. L. Engelstad, E. G. Lovell, G. T. Dao, and J. Zheng, "Mechanical analysis of hard pellicles for 157-nm lithography," Proc. of SPIE vol. 4346, 2001, pp. 1166-1174.

[33] D. Schmaljohann, Y. C. Bae, G. L. Weibel, A. H. Hamad, and C. K. Ober "Design strategies for 157-nm single-layer photoresists: lithographic evaluation of a poly(α -trifluoromethyl vinyl alcohol) copolymer," Proc. of SPIE vol. 3999, 2000, pp. 330-334.

[34] M.K. Crawford, A. E. Feiring, J. Feldman, R. H. French, M. P. Periyasamy, F. L. Schadt III, R.J. Smalley, F. C. Zumsteg, Jr., R. R. Kunz, V. Rao, L. Liao, and S. M. Holl, "New materials for 157-nm photoresists: characterization and properties," Proc. of SPIE vol. 3999, 2000, pp. 357-364.

[35] K. Patterson, M. Yamachika, R. J. Hung, C. J. Brodsky, S. Yamada, M. H. Somervell, B. Osborn, D. S. Hall, G. Dukovic, J. D. Byers, W. Conley, and C. G.

Willson, "Polymers for 157-nm photoresist applications: a progress report," Proc. of SPIE vol. 3999, 2000, pp. 365-374.

[36] R. H. French, R.C. Wheland, D.J. Jones, J. N. Hilfiker, R. A. Synowicki, F. C. Zumsteg, Jr., J. Feldman, and A. E. Feiring, "Fluoropolymers for 157-nm lithography: optical properties from VUV absorbance and ellipsometry measurements," Proc. of SPIE vol. 4000, 2000, pp. 1491-1502.

[37] H. Ito, G. M. Wallraff, N. Fender, P.J. Brock, W.D. Hinsberg, and A. Mahorowala, "Development of 157nm positive resists," J. Vac. Sci. technol.B. vol. 19, no. 6,1999, pp. 2678-2684.

[38] P. Jedrasik, "DOF Imporvement by complex pupli filtering for DUV lithography," Proc. of SPIE. vol. 3679, 1999, pp. 800- 811.

[39] P. Robertson, "Proximity Effects in Projection Lithography: A Case Study of the Perkin-Elmer Micralign." M.S. Thesis, U.C. Berkeley , 1981.

[40] D. Robertson, F.W. Wise, A.N. Nasr, A.R. Neureuther, and C.H. Ting, "Proximity effects and influences of nonuniform illumination in projection lithography" Proc. of SPIE. vol. 334, 1982, pp. 37-43.

[41] H. Kang, C. Kim, J. Lee, W. Han, and Y. Koh, "High performance lithography with advanced modified illumination," IEICE transactions on Electronics, vol. 77-C, no.3, 1994, pp.432-437.

[42] B. W. Smith, "Forbidden Pitch or Duty-Free: Revealing the Causes of Across-Fitch Imaging Differences," Proc. of SPIE vol. 5040, 2003, pp399-407.

[43] A. E. Rosenbluth, S. J. Bukofsky, M.S. Hibbs, K. Lai, A. F. Molless, R. N. Singh, and A. K. Wong., "Optimum mask and source patterns to print a given shape," Proc. of SPIE, vol. 4346, 2001, pp486-502.

[44] M. Levenson, N. Viswanathan, and R. Simpson, "Improving resolution in photolithography with phase shift mask," IEEE Transactions on Electron Devices, vol.29,no.12, 1982, pp. 1812-1846.

[45] S. Inoue, T. Fujisawa, S. Tanaka, S. Tamamushi, Y. Ogawa, and M. Nakase, "Phase contrast lithography," Proc. of SPIE. vol.1927,1993, pp. 521-532.

[46] T. Terasawa, N. Hasegawa, and H. Fukuda, "0.3um optical lithography using a phase shifting mask," Proc. of SPIE vol.1088,1989, pp. 25.

[47] K. Toh, G.Dao, R. Singh, and H.Gaw, "Chromeless Phase shifted mask: A new approach to phase shift masks," Proc. of SPIE vol.1496, 1990, pp.27-53.

[48] B.J. Lin, "The Attenuated PSM," Solid State technology 35,1992,pp. 43-47.

[49] T. Terazawa, N. Hasegawa, and H. Fukuda, "Imaging characteristics of multi-phase-shifting and half tone phase shifting masks," Jpn. J. of Appl. Phys., vol. 30. no. 11B, 1991, pp.2991-2997.

[50] H. Fujkuda, A. Imai, and S. Okazaki, "Phase shifting mask and flex method for advanced photolithography," Proc. Of SPIE. vol. 1264, 1990, pp. 14- 25.

[51] A. R. Neureuther and M. Li "Assessment of synchronous filtering as an alternative to phase shifting mask at k=0.4," Proc. Of SPIE vol. 3679, 1999, pp. 420.

[52] J. H. Bruning, "Optical lithography--thirty years and three orders of magnitude: the evolution of optical lithography tools," Proc. of SPIE vol. 3051, 1997, p. 14-27.

[53] B. J. Lin, "New lambda, NA scaling equations for resolution and depth-of-focus," , Proc. of SPIE vol.4000,2000, pp. 759-764.

[54] G. D. Hutcheson and J. D. Hutcheson, "Technology and Economics in the Semiconductor Industry," Scientific American, vol. 274, No. 1, 1996, pp. 54-62.

[55] T. Yamauchi, "Pelliclizing technology," Proc. of SPIE vol. 1496, 1991, pp. 302-314.

[56] C. Sheppard and H. Matthews, "Imaging in high-aperture optical systems," JOSA A 4, 1987, pp. 1354-1355.

[57] J. Bischoff and R. Brunner, "Numerial investigation of the resolution in solid immersion lens system," Proc. of SPIE vol.4099, 2000, pp. 235-245.

[58] D. G. Flagello, W. Arnold, S. Hansen, M. Dusa, R.Socha, J. Mullkens, and R. Garreis, "Optical lithography in the sub-50nm regime," Proc. of SPIE vol. 5377, 2004, pp. 21-33.

[59] F. Uesawa, M. Katsumata, K. Ogawa, K. Takeuchi, S. Omori, M. Yoshizawa, and H. Kawahira, "Lithography of choice for 45nm node: New medium, new waveleng or new beam," Proc. of SPIE vol. 5377, 2004, pp. 34-45.

[60] B. Streefkerk, J. Baselmans, W. Gehoel-van Ansem, J. Mullkens, C. Hoogendam, M. Hoogendorp, D. Flagello, H. Sewell, and P. Graeupner, "Extending optical lithography with immersion," Proc. of SPIE vol. 5377, 2004, pp. 285-305.

[61] A. Takanashi, T. Harada, M. Akeyama, Y. Kondo, T. Kurosaki, S. Kuniyoshi, S. Hosaka, Y. Kawamura, "Pattern forming apparatus", US Patent 4,480,910, 1984.

[62] B.W. Smith, H. Kang, A. Bourov, and P. Rack, "Optical research for UV and VUV SRC contract 775," SRC program review 2000.

[63] M. Switkes and M. Rothschild, "Immersion lithography at 157nm," J. Vac. Sci. technol.B. vol. 19, no. 6, 1999, pp. 2353- 2356.

[64] R. Fernandex-Prini, " Release on the refractive index of ordinary water substance as a function of wavelength, temperature and pressure," The international Association for the properties of water and steam, 1997, www.iapws.org.

[65] W. Tabarelli, E. W. Lobach, "Apparatus for the photolithographic manufacture of integrated circuit elements," US Patent 4,509,852, 1982.

[66] B.J. Lin, "Immersion lithography and its impact on semiconductor manufacturing," Proc. of SPIE vol. 5377, 2004, pp. 46-65.

[67] H. Kawata, J.M. Carter, A. Yen, and H.I. Smith, "Optical projection lithography using lenses with numerical aperture greater than unity," Microelectronic Engineering, Elsevier science publisher B.V. North Holland, vol.9, 1989, pp.31.

[68] P.L. Marston, "Light scattering from bubbles in water," Proc. Of Oceans 89, vol.4, 1989, pp1186.

[69] A. Ershov, H Besaudele, and P. Das, "Performance characterization of ultranarrow ArF laser for DUV lithography," Proc. of SPIE vol. 3679, 1999, pp. 1030- 1037.

[70] J. W. Goodman, Introduction to Fourier Optics, McGraw-Hill, 1968.

[71] J. D. Gaskill, Linear systems, Fourier transfoms, and optics, Wiley, 1978

[72] H. Kang and B. W. Smith, "Fabrication of small contact using practical pupil filtering," Proc. of SPIE. vol. 4000, 2000 , pp. 1086-1091.

[73] B. W. Smith and H. Kang, "Spatial frequency filtering in pellicle plane," Proc. of SPIE. vol. 4000, 2000, pp. 252-265.

[74] M. Born and W. Wolf, Principle of Optics, Pergamon press, Oxford, 1980.

[75] TFCALC user guide, Software Spectra, inc., Portland, OR.

[76] ASML Netherlands B.V., Veldhoven, Netherlands.

[77] Rohm and Haas microelectronic materials inc., North Andover, MA.

[78] J. A. R. Samson, " Techniques of Vacuum Ultraviolet spectroscopy," J. Wiley & Sons Inc., NewYork, 1967.

[79] Y. Uehara, W. Sasaki, S. Saito, E. Fujiwara, Y. Kato, M. Yamanaka, K. Tsuchida, and J. Fujita, "High power Argon excimer laser at 126nm pumped by an electron beam," Optics letter, vol. 9, no. 12, 1984, pp. 539-541.

[80] K. Kurosawa, W. Sasaki, M. Okuda, Y. Takikawa, K. Yoshita, E. Fujiwara, and Y. Kato, "Super polished silicon carbide mirror for high power operation of excimer lasers in a vacuum ultraviolet spectral range," Rev. Sci. Instrument, vol. 61, No. 2, 1990, pp. 728- 731.

[81] M. Katto, M. Okuda, W. Sasaki, K. Kurosawa, and Y. Kato, "Electron beam pumped argon excimer laserusing an unstable resornator," IEEE journal on selected topics in quantum electronics, vol. 1, no. 3, 1995, pp. 924-930.

[82] Y. Uehara, W. Sasaki, S. Kasai, S. Saito, E. Fujiwara, Y. Kato, C. Yamanaka, M. Yamanaka, K. Tsuchida, and J. Fujita, "Tunable oscillation of a high power argon excimer laser in the vacuum ultraviolet spectral region," Optics letter, vol. 10, No. 10,1985, pp. 487-489.

[83] W. Smith, Modern Optical Engineering, Mcgraw-hill,1990, pp. 415-416.

[84] Coherent inc, part number 25-2522, Santa Clara, CA.

[85] OSLO user's guide, Synoptics, Littleton, MA.

[86] R. F. Hollman, and D.Elliott, "Small field projection imaging system for deep UV development," Proc. of SPIE. vol. 2197, 1993, pp. 876- 881.

[87] D.C. Shavor, D.M. Craig,C.A. Marchi,M.A. Hartney, and F. Goodal, "A small field stepper for 193nm lithography process development," Proc. of SPIE. vol. 1674, 1992, pp. 766-775.

[88] ADE Technologies, Inc., Digital Measurement Systems, Westwood, MA.

[89] V. Rao, J. Hutchinson, S. Holl, and J. Langston, "Top surface imaging process and materials developemtn for 193nm and extreme ultraviolet lithography," J. Vac. Sci. technol.B. vol. 16, no. 6, 1998, pp. 3722- 3725.

[90] C. Mertesdorf, N. Münzel, H. Holzwarth, P. Falcigno, H. T. Schacht, O. Rohdem, R. Schulz, S. G. Slater, D. Frey, O. Nalamasu, A. G. Timko, and T. X. Neenan, "Structural Design of Ketal and Acetal Blocking Groups in 2-Component

Chemically Amplified Positive DUV-Resists," Proc. of SPIE vol. 2438, 1995, pp.84–98.

[91] H.Ito, 'The annealing concept for environmental stabilization of chemically amplified resists'. ACS symposium, Microelectonics Technology, 614, 1994, pp.21 –34.

[92] Arch Chemicals, Inc., Norwalk, CT.

[93] Tokyo Ohka Kogyo CO. Ltd., Tokyo, Japan.

[94] T.A. Bruner, N. Seong, W.D. Hinsberg, J.A. Hoffnangle, F.A. Houle, and M.I. Sanchez, "High numerical aperture lithography imagery at the Brewster angle," J.microlith. Microfab. Microsyst. vol. 1, 2002, pp.189.

[95] B.W. Smith and J. Cashmore, "Challenges in high NA polarization and photoresists," Proc. of SPIE vol. 4691, 2002, pp. 11-24.

[96] D. G. Flagello and T. D. Milster, "Experimental verification of high-numerical-aperture effects in photoresist," Proc. of SPIE vol. 2197, 1994, pp. 466-478.

[97] S. H. Zaida and S.R. Brueck, "Multiple exposure interferemetric lithography," J. Vac. Sci. technol.B. vol. 11, no. 3, 1993, pp. 658-666.

[98] A. Fernandez, H.T. Nguyen, J.A. Britten, R.D. Boyd, M.D. Perry, and D. R. Kania, "Use of interference lithography to pattern arrays of sub micron ressit structures for field emission flat panel display," J. Vac. Sci. technol.B. vol. 15, 1997, no. 3, pp. 729- 735.

[99] X. Chen and S.R. J. Brueck, "Imaging Interoferomteric lithography: a wavelength division multiplex approach to extending optical lithography," J. Vac. Sci. technol.B. vol. 16, no. 6, 1998, pp. 3392-3397.

[100] T.A. Savas, S. M. Shah, M.L. Schattenburg, J.M. Carter, and H. I. Smith, "Achromatic interference Lithography for 100nm period grating and gratings.," J. Vac. Sci. technol. B, vol.13, no. 6, 1995, pp. 2732 –2735.

[101] G. Fütterer, W. Herbst, J. Rottstegge, M. Ferstl, M.Sebald, and J. Schwider, "Interference patterning of gratings with a period of 150 nm at a wavelength of 157nm," Proc. of SPIE vol. 4691, 2002, pp. 1703-1713.

[102] M.Paulus, B. Michel, and O. J.F. Martin, "Near field distribution in light coupling masks for contrast lithography," J. Vac. Sci. technol.B. vol. 17, no. 6, 1999, pp. 3314- 3317.

[103] A. Maripov and Y. Ismanov, "Interferometer based on the Talbot effect in holography," J. Opt. 26 No. 1, 1995, pp. 25-28.

[104] B. Smith, A. Bourov, H. Kang, F. Corpanese, Y. Fan, N. Lafferty, and L. Zavialova, "Water immersion optical lithography at 193nm," J.microlith. Microfab. Microsyst. 3, 2004 , pp.44-51.

[105] Gam Laser, inc. Orlando, Fl.

[106] Brewer Science, Inc., Rolla, MO.

[107] Air Product inc., Allentown, PA.